Results in Physics 39 (2022) 105799

Contents lists available at ScienceDirect

Results in Physics

journal homepage: www.elsevier.com/locate/rinp

# Dynamical bifurcation of a sewage treatment model with general higher-order perturbation

Yassine Sabbar [a], Anwar Zeb [b,*], Driss Kiouach [a], Nadia Gul [c], Thanin Sitthiwirattham [d], Dumitru Baleanu [e], Jiraporn Pongsopa [f,*]

[a] LPAIS Laboratory, Faculty of Sciences Dhar El Mahraz, Sidi Mohamed Ben Abdellah University, Fez, Morocco
[b] Department of Mathematics, COMSATS University of Islamabad, Abbottabad Campus, Abbottabad, Khyber Pakhtunkhwa, Pakistan
[c] Department of Mathematics, Shaheed Benazir Bhutto Women University, Peshawar, 25000, Khyber Pakhtunkhwa, Pakistan
[d] Mathematics Department, Faculty of Science and Technology, Suan Dusit University, Bangkok 10300, Thailand
[e] Department of Mathematics, Faculty of Arts and Sciences, Cankaya University, TR-06530, Ankara, Turkey
[f] Physics Department, Faculty of Science and Technology, Suan Dusit University, Bangkok 10300, Thailand

ARTICLE INFO

*MSC:*
60H10
92B05

*Keywords:*
Chemostat model
Stochastic process
Dynamics
Wastewater
Higher-order perturbation

ABSTRACT

In this research, we expose new results on the dynamics of a high disturbed chemostat model for industrial wastewater. Due to the complexity of heavy and erratic environmental variations, we take into consideration the polynomial perturbation. We scout the asymptotic characterization of our proposed system with a general interference response. It is demonstrated that the long-run characteristics of the chemostat process are classified by using the threshold classification approach. If the critical sill is strictly negative, the bacteria will disappear exponentially, indicating that the chemostat wastewater process is not running (*excluded scenario*), otherwise, the stationarity and ergodicity properties of our model are verified (*practical scenario*). The theoretical arsenal of this work offers a comprehensive overview of the industrial wastewater behavior under general hypotheses and introduces novel technical aspects to deal with other perturbed systems in biology. Numerically, we audit the accuracy of our threshold in three particular situations: linear, quadratic and cubic perturbations. We establish that the increasing order of disturbance has a passive influence on the extinction time of bacteria. This finding highlights that complex noise sources fulfill a significant role in the transient dynamics of chemostat systems.

## Research background and methodology

A bacterial chemostat is a lab setup composed of three inter-joined containers that worked to breed and collect the bacteria in an appropriate biological environment [1,2]. In its customary format, the supply tank way out is the inlet of the culture vessel, while the exit of the latter is the inlet of the collecting bottle. The first bottle comprises all the alimentary elements that help to increase the bacteria. The content of this vessel is pumped into the second one at a stationary rate. The bacteria feed on nutrients from the alimentation vessel and live in the culture vessel which is well stirred so that all the organisms have similar access to the nutrients [3]. The content of the culture container is then pumped into the third vessel which includes nutrient sources, bacteria, and the bio-appendages produced by these bacteria [4].

Chemostat tool represents the usual exemplification of the physical and biological rivalry that exists when two or more groups compete for the same nourishment supply [5]. It carries out a pivotal role in the theoretical ecology [1], population dynamics [2], chemical domains [6], industrial treatments [7], biochemical development [8], and other areas. Chemostat is also used in wastewater treatment and thanks to it we can transform wastewater into treated water which is reused in daily activities [9,10]. In general, wastewater is full of bacterial contaminants, chemicals, and other toxins that can result from industrial production and standard human activities. Its treatment process aims to reduce pollutants to reasonable levels and make the water safe to discharge back into the environment [11]. Fig. 1 presents a typical configuration and arrangement for a traditional process that is employed in the wastewater treatment [12]. Firstly, the wastewater flows through a sieve that clogs bulky solid objects such as human and industrial waste employing a specially designed robotic shovel. The sewage channel extends to the sedimentation zone, slowing down the velocity of the incoming sewage and thus allowing coarse particles such as gravel and sand, which are heavier than water, to settle to the

* Corresponding authors.
*E-mail addresses:* yassine.sabbar@usmba.ac.ma (Y. Sabbar), anwar@cuiatd.edu.pk (A. Zeb), d.kiouach@uiz.ac.ma (D. Kiouach), nadia.gul@sbbwu.edu.pk (N. Gul), thanin_sit@dusit.ac.th (T. Sitthiwirattham), dumitru@cankaya.edu.tr (D. Baleanu), jiraporn_pon@dusit.ac.th (J. Pongsopa).

https://doi.org/10.1016/j.rinp.2022.105799
Received 31 May 2022; Received in revised form 28 June 2022; Accepted 4 July 2022
Available online 7 July 2022

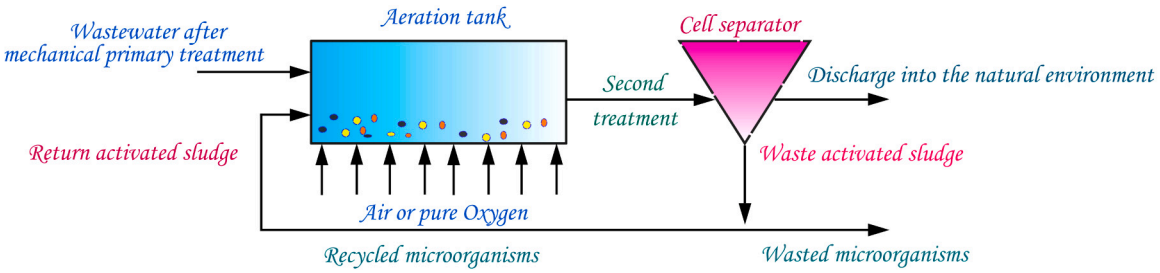


**Fig. 1.** A standard setting of the unit of the sewage treatment. The process consists of two main stages: the mechanical stage and the biological purification stage with the elimination of nutrients and microorganisms.

bottom of the stream [13]. In the first treatment basin, the filtered water is kept for 120 minutes. In this large rectangular tank, elusive suspended particles can settle as sludge at the bottom. This raw sludge is removed, condensed and transported to a digestion tank. The fat is discarded from light particles floating on the surface of the water such as industrial fats and oils and drained into a separate tank. The previous three operations constitute the first liquidation stage. Since it involves a purely mechanical and hydraulic treatment of waste water, it is also referred to as the mechanical treatment stage. This stage eliminates approximately 30 percent of the pollutants from the raw effluent wastewater that the plant has to treat in aggregate. In the biological treatment stage, a chemical process is used by passing the sewage liquid into the aeration tank. During the activated sludge process, oxygen is introduced into the liquid to generate conditions for microorganisms that feed on organic molecules dissolved in chemical and effluents. A large number of microorganisms form colonies that become visible as lumps of slime. These sludge clumps settle to the bottom of the secondary settling tank or filter device and are either returned to the activated sludge process or pumped into the primary settling tank for sludge disposal. Thus, removing sewage sludge from effluent removes degradable pollutants. Small sewage treatment plants frequently use drip filters, which are circular concrete tanks filled with porous rock that provide the large surface area that bacteria need to settle. It forms a continuous film ("bio-membrane"—it can be compared to a sludge conglomerate for the activated sludge process) through which the effluent passes. The mechanical and biological treatment stages clean the effluent by approximately 97% [14].

Mathematical modeling makes it possible to predict the asymptotic behavior of wastewater treatment processes according to operating and control parameters [15–17]. Mathematical models could be used to maximize the production of renewable energy from waste in the form of biogas which is mainly transformed into heat and electricity. For the reuse of water in agriculture in semi-arid regions, wastewater treatment uses biological depollution. The micro-organisms (or "biomass") transform the material (or substrate) present in the waste into organic form. Thus, the treatment uses microbial ecosystems to concentrate the pollution that should be optimized and controlled by identifying appropriate mathematical models. The chemostat is used as a starting point and plays an important role as a model in mathematical biology for wastewater treatment processes.

To mathematically describe the dynamics of bacteria (microorganisms) at the biological purification stage by using the chemostat approach, we consider a bacterial growth model in which the cell mass $\mathbf{M}$ grows through the consumption of a substrate species $\mathbf{N}$. The objective is to monitor the substrate and bacterial densities of wastewater generated by industrial activities. In this regard, Nguyen et al. in [18] proposed a chemostat wastewater model which takes the following form:

$$\begin{cases} \mathrm{d}\mathbf{N}(t) = \left\{ \frac{1}{\theta}\left(N_\star - \mathbf{N}(t)\right) - \frac{\mathfrak{b}\mathbf{N}(t)\mathbf{M}(t)}{1+\mathfrak{K}_{\mathbf{N}}\mathbf{N}(t)} \right\} \mathrm{d}t, \\ \mathrm{d}\mathbf{M}(t) = \left\{ \frac{\mathfrak{b}\mathbf{N}(t)\mathbf{M}(t)}{1+\mathfrak{K}_{\mathbf{N}}\mathbf{N}(t)} - \left(\mathcal{Q}_d + \frac{1+R_c}{\theta}\right)\mathbf{M}(t) \right\} \mathrm{d}t, \\ \mathbf{N}(0) > 0, \quad \mathbf{M}(0) > 0, \end{cases} \tag{1.1}$$

where $\mathbf{N}(t)$ and $\mathbf{M}(t)$ are the densities of the nourishing elements and the microbial organisms at time $t$ respectively. $\theta$ is the hydraulic retention time. $N_\star$ is the alimentation flux rate. $\mathfrak{b}$ indicates the highest rate of nutrient exhaustion and also the qualitative growing rate of $\mathbf{M}(t)$. $\mathcal{Q}_d$ represents the death ratio of $\mathbf{M}$. $R_c$ is the recycle percentage and $\mathfrak{K}_{\mathbf{N}}$ is the saturation constant of $\mathbf{N}$. For simplicity, we let $\mathcal{Q}_0 = \frac{1}{\theta}$ and $\mathcal{Q}_1 = \left(\mathcal{Q}_d + \frac{1+R_c}{\theta}\right)$.

When dealing with wastewater process, other properties should be included like the sensitivity of bacteria to nutrient concentrations and the biological interference between the chemostat components [19–21]. Therefore, the choice of the functional response affects the behavior of wastewater operation dynamics [22,23]. For this purpose, the present work puts forward a new chemostat wastewater system with an interference function that includes many types of responses. In line with this framework, the system (1.1) can be rewritten as follows:

$$\begin{cases} \mathrm{d}\mathbf{N}(t) = \left\{ \mathcal{Q}_0\left(N_\star - \mathbf{N}(t)\right) - \mathfrak{b}\mathcal{G}\left(\mathbf{N}(t),\mathbf{M}(t)\right)\mathbf{M}(t) \right\} \mathrm{d}t, \\ \mathrm{d}\mathbf{M}(t) = \left\{ \mathfrak{b}\mathcal{G}\left(\mathbf{N}(t),\mathbf{M}(t)\right)\mathbf{M}(t) - \mathcal{Q}_1\mathbf{M}(t) \right\} \mathrm{d}t, \\ \mathbf{N}(0) > 0, \quad \mathbf{M}(0) > 0. \end{cases} \tag{1.2}$$

To properly analyze this biological model, we assume that the general interference function $\mathcal{G} \in \mathcal{C}^2(\mathbb{R}_+ \times \mathbb{R}_+, \mathbb{R}_+)$ satisfies these two main assumptions:

- $\mathbf{A_a}$: $\mathcal{G}(0,\mathbf{M}) = 0$ $\forall \mathbf{M} \geq 0$; $\mathcal{G}$ is increasing in $\mathbf{N}$ and decreasing in $\mathbf{M}$; and there exists a positive constant $\varpi$ such that $\frac{\partial \mathcal{G}(\mathbf{N},\mathbf{M})}{\partial \mathbf{N}} \leq \varpi$, for all $\mathbf{N},\mathbf{M} \geq 0$.
- $\mathbf{A_b}$: $\lim\limits_{\mathbf{M}\to 0_{\mathbf{N}>0}} \sup\left\{ |\mathcal{G}(\mathbf{N},\mathbf{M}) - \mathcal{G}(\mathbf{N},0)| \right\} = 0$.

The properties $\mathbf{A_a}$ and $\mathbf{A_b}$ are naturally verified in the case of the typical examples listed in Table 1.

Stochastic calculus applied in biology represents a booming area of research that merges probabilities, differential equations, and mathematical modeling [24–29]. This amalgamation aims to supply an insight into micro-organisms dynamics under certain external fluctuations [30–32]. Changes in lab conditions, temperature, lighting, pressure and human intervention are concrete examples of factors influencing species dynamics [33–36]. To characterize this randomness, several analytical methods have been employed to extract information and predict the future of the studied phenomenon [37–39]. One such approach claims that stochastic fluctuations can be formulated by integrating white noises into the underlying model [40]. By considering this type of perturbations in its linear form, stochastic models have been adopted extensively in epidemiology to examine the propagation of the diseases [41–43], and in ecology to predict the long-time behavior of the species [44,45]. In both cases, the core objective was the discussion of some long-run properties such as: eradication and continuation of the population [46], stationarity and periodicity [47], stability and bifurcation analysis [48], etc.

Based on the fact that intense amounts of extrinsic fluctuations can strongly affect population dynamics, Liu and Jiang [49] proposed a new version of stochastic models. They showed that due to the

**Table 1**
List of some prototypes of the general interference function $\mathcal{G}$.

| Name | Expression |
|---|---|
| Functional response type 1 | $\mathcal{G}(\mathbf{N},\mathbf{M}) = \mathbf{N}$ |
| Functional response type 2 | $\mathcal{G}(\mathbf{N},\mathbf{M}) = \dfrac{\mathbf{N}}{\mathfrak{K}_{\mathbf{N}}+\mathbf{N}}$, $(\mathfrak{K}_{\mathbf{N}}>0)$ |
| Functional response type 3 | $\mathcal{G}(\mathbf{N},\mathbf{M}) = \dfrac{\mathbf{N}^2}{(\mathfrak{K}_{\mathbf{N}}+\mathbf{N})(\mathfrak{K}^{\star}_{\mathbf{N}}+\mathbf{N})}$, $(\mathfrak{K}_{\mathbf{N}},\mathfrak{K}^{\star}_{\mathbf{N}}>0)$ |
| Beddington–DeAngelis | $\mathcal{G}(\mathbf{N},\mathbf{M}) = \dfrac{\mathbf{N}}{1+\mathfrak{K}_{\mathbf{N}}\mathbf{N}+\mathfrak{K}_{\mathbf{M}}\mathbf{M}}$, $(\mathfrak{K}_{\mathbf{N}},\mathfrak{K}_{\mathbf{M}}>0)$ |
| Crowley–Martin | $\mathcal{G}(\mathbf{N},\mathbf{M}) = \dfrac{\mathbf{N}}{(\mathfrak{K}_{\mathbf{N}}+\mathbf{N})(\mathfrak{K}_{\mathbf{M}}+\mathbf{M})}$, $(\mathfrak{K}_{\mathbf{N}},\mathfrak{K}_{\mathbf{M}}>0)$ |
| Modified Crowley–Martin | $\mathcal{G}(\mathbf{N},\mathbf{M}) = \dfrac{\mathbf{N}}{1+\mathfrak{K}_{\mathbf{N}}\mathbf{N}+\mathfrak{K}_{\mathbf{M}}\mathbf{M}+\mathfrak{K}_{\mathbf{NM}}\mathbf{NM}}$, $(\mathfrak{K}_{\mathbf{N}},\mathfrak{K}_{\mathbf{M}},\mathfrak{K}_{\mathbf{NM}}>0)$ |

**Table 2**
Some studies on the dynamics of biological models with quadratic perturbation.

| Source | Biological model | Studied properties |
|---|---|---|
| [50] | Multi-stage HIV system | Stationarity and extinction |
| [51] | SICA-HIV system | Stationarity and ergodicity |
| [52] | General SIRS system | Stationarity and extinction |
| [53] | Epidemic model with relapse | Periodicity and stationarity |
| [54] | AIDS system with enhanced hypotheses | Stationarity and extinction |
| [55] | Multi staged HIV-AIDS system | Stationarity and extinction |
| [56] | Epidemic model with media intervention | Ergodicity and extinction |
| [57] | Impulsive chemostat system | Stationarity and extinction |
| [58] | Predator–prey system | Stationarity and ergodicity |
| [59] | Logistic equation with continuous delay | Stationarity and extinction |
| [60] | Standard SIR system | Periodicity and ergodicity |
| [61] | Switched Lotka–Volterra system | Ergodic property |
| [62] | Ecological system with additional food | Stationarity and extinction |
| [63] | HIV system | Extinction and stationarity |
| [64] | Hybrid stochastic SEQIHR epidemic model | Extinction and stationarity |

complexity of environmental variations, the order of the disturbance can be elevated to the second one. That is, the densities of individuals in the probabilistic part can depend on their squares next to the linear noise. This form of disturbance adopts many names such as higher order; second-order and non-linear perturbation. To unify these various names and for the convenience of readers, in this research, we call it quadratic fluctuations. In [49], the authors studied the stationarity and extinction properties of a classical SIR model with quadratic fluctuations. After that, scientific papers began to appear one by one adopting the similar idea with diverse applications and contexts. In order to offer an overview of the existing studies, we gather in Table 2 some biological models with quadratic fluctuations.

In *2021*, Zhou et al. [65] proposed the polynomial perturbation by implementing the Taylor expansion. This framework extends the aforementioned studies and provides a general setting of randomness. In line with this alternative representation, the current study aims to probe the impact of a complex polynomial perturbation on the long-term behavior of a chemostat wastewater system. Focusing on the unpredictability of bacteria interactions and the complexity of nature's random variations, we present the following stochastic chemostat model with polynomial perturbations:

$$\begin{cases} \mathrm{d}\mathbf{N}(t) = \overbrace{\left\{\mathcal{Q}_0\big(N_\star-\mathbf{N}(t)\big)-\mathfrak{b}\mathcal{G}\big(\mathbf{N}(t),\mathbf{M}(t)\big)\mathbf{M}(t)\right\}\mathrm{d}t}^{\text{Deterministic part}} \\ \qquad\qquad + \overbrace{\sum_{h=0}^{H}\mathfrak{m}_{1h}\mathbf{N}^{h+1}(t)\mathrm{d}\mathbf{W}_1(t)}^{\text{Polynomial perturbation}}, \\ \mathrm{d}\mathbf{M}(t) = \left\{\mathfrak{b}\mathcal{G}\big(\mathbf{N}(t),\mathbf{M}(t)\big)\mathbf{M}(t)-\mathcal{Q}_1\mathbf{M}(t)\right\}\mathrm{d}t + \sum_{h=0}^{H}\mathfrak{m}_{2h}\mathbf{M}^{h+1}(t)\mathrm{d}\mathbf{W}_2(t), \end{cases} \tag{1.3}$$

where $\mathbf{W}_1(t)$, $\mathbf{W}_2(t)$ are two independent Wiener processes defined on a filtered probability space $\Omega^{\mathcal{E},\mathbb{P}} \equiv (\Omega,\mathcal{E},\{\mathcal{E}_t\}_{t\geq 0},\mathbb{P})$ such that $\{\mathcal{E}_t\}_{t\geq 0}$ follows the usual assumptions, and $\mathfrak{m}_{kh} > 0$ $(k=1,2)$ $(h = 0,1,2,\ldots,N)$ are the polynomial order random intensities. Plainly, the random component at $H=0$ is the standard linear noise form adopted by many researchers. If $H=1$, it denotes the quadratic-order random perturbation situation. If $H=2$, it denotes the random perturbation with cubic order and so on.

Analytically speaking, the authors of [65] explored the long-run attitude of an epidemic system with polynomial fluctuations. But their suggested theoretical method has some restrictions and limitations, particularly since they offered two distinct critical values for extinction and stationarity, which is not ideal when dealing with biological systems. Furthermore, they pointed out that there is a critical gap between the established criteria, and that obtaining the corresponding global sill remains an open question (for more details, see the discussion part of [65]). In this research, we address this problem from a different angle by providing the sill value among the said asymptotic characteristics of the chemostat model (1.3), and this is the significant contribution of our analysis besides generalizing the functional response.

Technically, our new approach focuses on some characteristics of the Markov process $\mathbf{U}(t)$ that satisfies:

$$\mathrm{d}\mathbf{U}(t) = \Big(\mathcal{Q}_0 N_\star - \mathcal{Q}_0\mathbf{U}(t)\Big)\mathrm{d}t + \sum_{h=0}^{H}\mathfrak{m}_{1h}\mathbf{U}^{h+1}(t)\mathrm{d}\mathbf{W}_1(t), \qquad \mathbf{U}(0)=\mathbf{N}(0).$$

In accordance with Lemma 5 of [65], $\mathbf{U}$ admits the single steady distribution $\pi^{\mathbf{U}}(y) = \Pi\left(\sum_{h=0}^{H}\mathfrak{m}_{1h}y^{h+1}(t)\right)^{-2} e^{2\eta(y)}$, where

$$\eta(y) = \int_{\frac{\mathcal{Q}_0 N_\star}{\mathfrak{u}+\mathfrak{z}}}^{y}\big(\mathcal{Q}_0 N_\star - \mathcal{Q}_0\tau\big)\left(\sum_{h=0}^{H}\mathfrak{m}_{1h}\tau^{h+1}(t)\right)^{-2}\mathrm{d}\tau,$$

and $\Pi$ is a specific constant that verifies $\int_{\mathbb{R}_+}\pi^{\mathbf{U}}(y)\mathrm{d}y = 1$. From the probabilistic comparison result [66], we can compare the processes $\mathbf{U}$ and $\mathbf{N}$ as follows: $\mathbf{U}(t)\geq\mathbf{N}(t)$ almost surely (a.s.). Furthermore, the time average of $\mathbf{U}(t)$ converges almost surely to $\int_{\mathbb{R}_+} y\pi^{\mathbf{U}}(\mathrm{d}y)$ as $t\to\infty$. In consonance with the above results, we clearly point out that the present

work aims to prove that the following quantity:

$$\mathfrak{R}_{\star}^{\Sigma}=\mathfrak{b}\int_{\mathbb{R}_{+}}\mathcal{G}(y,0)\pi^{\mathbf{U}}(\mathrm{d}y)-\mathcal{Q}_{1}-0.5\mathfrak{m}_{20}^{2},$$

is the sill among the disappearance and ergodicity of **M** by the use of the probabilistic comparison theorem, the exponential inequality for martingales, the Feller property and other mathematical tools. The obtained threshold value $\mathfrak{R}_{\star}^{\Sigma}$ is regarded to be sufficient for having an excellent view of the long-time chemostat process. Specifically, if $\mathfrak{R}_{\star}^{\Sigma}>0$, we have the existence and uniqueness of an ergodic stationary distribution, while the extinction happens when $\mathfrak{R}_{\star}^{\Sigma}<0$.

The remainder of this research is ordered as the following arrangement: in the section "Dynamical bifurcation of the stochastic system (1.3)", we deal with the dynamical bifurcation by demonstrating that $\mathfrak{R}_{\star}^{\Sigma}$ is the real threshold of our system (1.3). In the section "Numerical experiment: Industrial wastewater treatment", we numerically verify the correctness of our results in three particular situations: linear, quadratic, and cubic perturbations. Finally, we discuss our theoretical and numerical results.

## Dynamical bifurcation of the stochastic system (1.3)

### *Scenario 1: Disappearance of bacteria*

This subsection aims to exhibit the criterion for the demise of the bacteria **M**.

**Theorem 2.1.** *Let* $(\mathbf{N}(t),\mathbf{M}(t))$ *be the unique solution of system* (1.3) *with any initial value* $(\mathbf{N}(0),\mathbf{M}(0))\in\mathbb{R}_{+}^{2,\star}$. *If* $\mathfrak{R}_{\star}^{\Sigma}<0$, *then*

$$\limsup_{t\to\infty}t^{-1}\ \ln\mathbf{M}(t)\leq\mathfrak{R}_{\star}^{\Sigma}<0\quad\text{a.s.},$$

*which means that the bacteria* **M** *will exponentially die out with probability one. In addition, the distribution of the nutrient* $\mathbf{N}(t)$ *converges weakly to the stationary distribution* $\pi^{\mathbf{U}}$ *of* $\mathbf{U}(t)$.

**Proof.** This demonstration is divided into two parts.

*Part I.* By using the Itô's formula, we get

$$\begin{aligned}\mathrm{d}\ln\mathbf{M}(t)&=\left(\mathfrak{b}\mathcal{G}(\mathbf{N}(t),\mathbf{M}(t))-\mathcal{Q}_{1}-0.5\left(\sum_{h=0}^{H}\mathfrak{m}_{2h}\mathbf{M}^{h}(t)\right)^{2}\right)\mathrm{d}t\\&\quad+\sum_{h=0}^{H}\mathfrak{m}_{2h}\mathbf{M}^{h}(t)\mathrm{d}\mathbf{W}_{2}(t).\end{aligned}$$

In line with the probabilistic comparison lemma ($\mathbf{U}(t)\geq\mathbf{N}(t)$ a.s.), we obtain

$$\begin{aligned}\mathrm{d}\ln\mathbf{M}(t)&\leq\left(\mathfrak{b}\mathcal{G}(\mathbf{U}(t),0)-\mathcal{Q}_{1}-0.5\left(\sum_{h=0}^{H}\mathfrak{m}_{2h}\mathbf{M}^{h}(t)\right)^{2}\right)\mathrm{d}t\\&\quad+\sum_{h=0}^{H}\mathfrak{m}_{2h}\mathbf{M}^{h}(t)\mathrm{d}\mathbf{W}_{2}(t).\end{aligned}\tag{2.1}$$

We make two operations on both sides of (2.1): integration from 0 to $t$ and division by $t$, then

$$\begin{aligned}&t^{-1}\ln\mathbf{M}(t)-t^{-1}\ln\mathbf{M}(0)\\&\leq t^{-1}\mathfrak{b}\int_{0}^{t}\mathcal{G}(\mathbf{U}(\tau),0)\mathrm{d}\tau-\mathcal{Q}_{1}\\&\quad+t^{-1}\underbrace{\left(\int_{0}^{t}\sum_{h=0}^{H}\mathfrak{m}_{2h}\mathbf{M}^{h}(\tau)\mathrm{d}\mathbf{W}_{2}(\tau)-0.5\int_{0}^{t}\left(\sum_{h=0}^{H}\mathfrak{m}_{2h}\mathbf{M}^{h}(\tau)\right)^{2}\mathrm{d}\tau\right)}_{=\mathcal{K}(t)}.\end{aligned}\tag{2.2}$$

Based on the use of the exponential inequality for martingales [67], we get

$$\begin{aligned}&\mathbb{P}\left\{\sup_{t\in[0,T_{1}]}\left(\int_{0}^{t}\sum_{h=0}^{H}\mathfrak{m}_{2h}\mathbf{M}^{h}(\tau)\mathrm{d}\mathbf{W}_{2}(\tau)\right.\right.\\&\left.\left.-0.5\alpha_{1}\int_{0}^{t}\left(\sum_{h=0}^{H}\mathfrak{m}_{2h}\mathbf{M}^{h}(\tau)\right)^{2}\mathrm{d}\tau\right)>\frac{2\ln T_{1}}{\alpha_{1}}\right\}\leq T_{1}^{-2},\end{aligned}$$

for all $0<\alpha_{1}<1$ and $T_{1}>0$. From the Borel–Cantelli result [67], we assure the existence of $T_{1,\omega}=T_{1}(\omega)$, $\forall\omega$ in $\Omega$ such that the inequality

$$\int_{0}^{t}\sum_{h=0}^{H}\mathfrak{m}_{2h}\mathbf{M}^{h}(\tau)\mathrm{d}\mathbf{W}_{2}(\tau)\leq\frac{2\ln T_{1}}{\alpha_{1}}+0.5\alpha_{1}\int_{0}^{t}\left(\sum_{h=0}^{H}\mathfrak{m}_{2h}\mathbf{M}^{h}(\tau)\right)^{2}\mathrm{d}\tau,$$

holds for all $T_{1}\geq T_{1,\omega}$ and $T_{1}-1<t\leq T_{1}$ a.s. Under this setting, we have

$$\begin{aligned}t^{-1}\mathcal{K}(t)&\leq\frac{2\ln T_{1}}{\alpha_{1}t}+t^{-1}0.5\alpha_{1}\int_{0}^{t}\left(\sum_{h=0}^{H}\mathfrak{m}_{2h}\mathbf{M}^{h}(\tau)\right)^{2}\mathrm{d}\tau\\&\quad-t^{-1}0.5\int_{0}^{t}\left(\sum_{h=0}^{H}\mathfrak{m}_{2h}\mathbf{M}^{h}(\tau)\right)^{2}\mathrm{d}\tau\\&\leq\frac{2\ln T_{1}}{\alpha_{1}(T_{1}-1)}-t^{-1}0.5(1-\alpha_{1})\int_{0}^{t}\left(\sum_{h=0}^{H}\mathfrak{m}_{2h}\mathbf{M}^{h}(\tau)\right)^{2}\mathrm{d}\tau\\&\leq\frac{2\ln T_{1}}{\alpha_{1}(T_{1}-1)}-0.5(1-\alpha_{1})\mathfrak{m}_{20}^{2}.\end{aligned}$$

We take the superior limit on two sides of (2.2), then

$$\begin{aligned}\limsup_{t\to\infty}t^{-1}\ln\mathbf{M}(t)&\leq\mathfrak{b}\lim_{t\to\infty}t^{-1}\int_{0}^{t}\mathcal{G}(\mathbf{U}(\tau),0)\mathrm{d}\tau-\mathcal{Q}_{1}+\lim_{t\to\infty}t^{-1}\mathcal{G}(t)\\&\leq\mathfrak{b}\int_{\mathbb{R}_{+}}\mathcal{G}(y,0)\pi^{\mathbf{U}}(\mathrm{d}y)-\mathcal{Q}_{1}\\&\quad+\lim_{T_{1}\to\infty}\frac{2\ln T_{1}}{\alpha_{1}(T_{1}-1)}-0.5(1-\alpha_{1})\mathfrak{m}_{20}^{2}\\&=\mathfrak{b}\int_{\mathbb{R}_{+}}\mathcal{G}(y,0)\pi^{\mathbf{U}}(\mathrm{d}y)-\mathcal{Q}_{1}-0.5(1-\alpha_{1})\mathfrak{m}_{20}^{2}\quad\text{a.s.}\end{aligned}$$

We let $\alpha_{1}$ tends to $0^{+}$, then the obtained result is

$$\limsup_{t\to\infty}t^{-1}\ln\mathbf{M}(t)\leq\mathfrak{R}_{\star}^{\Sigma}<0\quad\text{a.s.}$$

Since the exponential disappearance of the bacteria implies the almost surely extinction, then $\lim_{t\to\infty}\mathbf{M}(t)=0$ a.s. In other words, the bacteria in the chemostat of (1.3) will go to extinction with probability one.

*Part II.* Based on the result of Part I, we can conclude that for a small $\mathfrak{r}>0$, we have the existence of $\mathfrak{t}_{0}$ and $\Omega_{\mathfrak{r}}\subset\Omega$ such that $\mathbb{P}(\Omega_{\mathfrak{r}})>1-\mathfrak{r}$ and

$$\mathcal{G}(\mathbf{N},\mathbf{M})\mathbf{M}\leq\mathcal{G}(\mathbf{N},0)\mathbf{M}\leq\varpi\mathfrak{r}\mathbf{N}.$$

Thus

$$\begin{aligned}&\left(\mathcal{Q}_{0}\left(N_{\star}-\mathbf{N}(t)\right)-\mathfrak{b}\varpi\mathfrak{r}\mathbf{N}(t)\right)\mathrm{d}t+\sum_{h=0}^{H}\mathfrak{m}_{1h}\mathbf{N}^{h+1}(t)\mathrm{d}\mathbf{W}_{1}(t)\\&\leq\mathrm{d}\mathbf{N}(t)\leq\left(\mathcal{Q}_{0}\left(N_{\star}-\mathbf{N}(t)\right)\right)\mathrm{d}t+\sum_{h=0}^{H}\mathfrak{m}_{1h}\mathbf{N}^{h+1}(t)\mathrm{d}\mathbf{W}_{1}(t),\end{aligned}$$

indicates that the distribution of $\mathbf{N}(t)$ converges weakly to $\pi^{\mathbf{U}}(\cdot)$. The proof of the extinction theorem is finished. □

### *Scenario 2: Continuation of bacteria*

This subsection introduces a new approach to establish the condition of the existence of the unique ergodic stationary distribution of our system (1.3).

**Theorem 2.2.** *For any initial data* $\big(\mathbf{N}(0),\mathbf{M}(0)\big)\in\mathbb{R}_+^{2,\star}$, *if* $\mathfrak{R}_\star^\Sigma>0$, *the solution* $\big(\mathbf{N}(t),\mathbf{M}(t)\big)$ *to system* (1.3) *has the ergodic property and admits a unique stationary distribution* $\pi^\Sigma(\cdot)$.

**Proof.** For plainness and clarity, we set

$$\left(\sum_{h=0}^{H}\mathfrak{m}_{2h}\mathbf{M}^h(t)\right)^2=\sum_{h=0}^{2H}\underbrace{\left(\sum_{j+k=h}\mathfrak{m}_{2j}\mathfrak{m}_{2k}\right)}_{\mathfrak{u}_h}\mathbf{M}^h(t)=\sum_{h=0}^{2H}\mathfrak{u}_h\mathbf{M}^h(t).$$

Via using Itô's formula, one obtains

$$\begin{aligned}\mathcal{L}\Big(-\ln\mathbf{M}(t)\Big)&=-\mathfrak{b}\mathcal{G}\big(\mathbf{N}(t),\mathbf{M}(t)\big)+\mathcal{Q}_1+0.5\left(\sum_{h=0}^{H}\mathfrak{m}_{2h}\mathbf{M}^h(t)\right)^2\\&=-\mathfrak{b}\mathcal{G}\big(\mathbf{U}(t),0\big)+\mathfrak{b}\mathcal{G}\big(\mathbf{U}(t),0\big)-\mathfrak{b}\mathcal{G}\big(\mathbf{N}(t),0\big)\\&\quad+\mathfrak{b}\mathcal{G}\big(\mathbf{N}(t),0\big)-\mathfrak{b}\mathcal{G}\big(\mathbf{N}(t),\mathbf{M}(t)\big)\\&\quad+\mathcal{Q}_1+0.5\mathfrak{m}_{20}^2+\mathfrak{m}_{20}\mathfrak{m}_{21}\mathbf{M}(t)+0.5\sum_{h=2}^{2H}\mathfrak{u}_h\mathbf{M}^h(t).\end{aligned}$$

From assumption $\mathbf{A_a}$, we have

$$\begin{aligned}\mathcal{L}\Big(-\ln\mathbf{M}(t)\Big)&\le-\mathfrak{b}\mathcal{G}\big(\mathbf{U}(t),0\big)+\mathcal{Q}_1+0.5\mathfrak{m}_{20}^2+\mathfrak{b}\varpi\big(\mathbf{U}(t)-\mathbf{N}(t)\big)\\&\quad+\mathfrak{b}\mathcal{G}\big(\mathbf{N}(t),0\big)-\mathfrak{b}\mathcal{G}\big(\mathbf{N}(t),\mathbf{M}(t)\big)+\mathfrak{m}_{20}\mathfrak{m}_{21}\mathbf{M}(t)\\&\quad+0.5\sum_{h=2}^{2H}\mathfrak{u}_h\mathbf{M}^h(t).\end{aligned}\tag{2.3}$$

On the other hand, we get

$$\begin{aligned}\mathcal{L}\Big(\ln\mathbf{U}(t)-\ln\mathbf{N}(t)\Big)&\le\mathcal{Q}_0N_\star\Big(\mathbf{U}^{-1}(t)-\mathbf{N}^{-1}(t)\Big)\\&\quad+\mathfrak{b}\mathcal{G}\big(\mathbf{N}(t),\mathbf{M}(t)\big)\mathbf{M}(t)\mathbf{N}^{-1}(t)\\&\quad-0.5\left(\sum_{h=0}^{H}\mathfrak{m}_{1h}\mathbf{U}^h(t)\right)^2+0.5\left(\sum_{h=0}^{H}\mathfrak{m}_{1h}\mathbf{N}^h(t)\right)^2.\end{aligned}$$

Since $\mathbf{U}(t)\ge\mathbf{N}(t)$ a.s., we obtain

$$\mathcal{L}\Big(\ln\mathbf{U}(t)-\ln\mathbf{N}(t)\Big)\le-\mathfrak{m}_{10}\mathfrak{m}_{11}\big(\mathbf{U}(t)-\mathbf{N}(t)\big)+\mathfrak{b}\varpi\mathbf{M}(t).\tag{2.4}$$

We consider a function $f(t)$ expressed by

$$f(t)=-\ln\mathbf{M}(t)+\frac{\mathfrak{b}\varpi}{\mathfrak{m}_{10}\mathfrak{m}_{11}}\Big(\ln\mathbf{U}(t)-\ln\mathbf{N}(t)\Big).$$

Based on (2.3) and (2.4), we get

$$\begin{aligned}\mathcal{L}f(t)&\le-\mathfrak{b}\mathcal{G}\big(\mathbf{U}(t),0\big)+\mathcal{Q}_1+0.5\mathfrak{m}_{20}^2+\left(\mathfrak{m}_{20}\mathfrak{m}_{21}+\frac{\mathfrak{b}^2\varpi^2}{\mathfrak{m}_{10}\mathfrak{m}_{11}}\right)\mathbf{M}(t)\\&\quad+0.5\sum_{h=2}^{2H}\mathfrak{u}_h\mathbf{M}^h(t)+\mathfrak{b}\mathcal{G}\big(\mathbf{N}(t),0\big)-\mathfrak{b}\mathcal{G}\big(\mathbf{N}(t),\mathbf{M}(t)\big).\end{aligned}\tag{2.5}$$

We add and subtract at the same time the quantity $\mathfrak{b}\int_{\mathbb{R}_+}\mathcal{G}(y,0)\pi^{\mathbf{U}}(\mathrm{d}y)$ in (2.5) as follows:

$$\begin{aligned}\mathcal{L}f(t)&\le-\mathfrak{b}\int_{\mathbb{R}_+}\mathcal{G}(y,0)\pi^{\mathbf{U}}(\mathrm{d}y)+\mathcal{Q}_1+0.5\mathfrak{m}_{20}^2\\&\quad+\mathfrak{b}\left(\int_{\mathbb{R}_+}\mathcal{G}(y,0)\pi^{\mathbf{U}}(\mathrm{d}y)-\mathcal{G}\big(\mathbf{U}(t),0\big)\right)\\&\quad+\left(\mathfrak{m}_{20}\mathfrak{m}_{21}+\frac{\mathfrak{b}^2\varpi^2}{\mathfrak{m}_{10}\mathfrak{m}_{11}}\right)\mathbf{M}(t)+0.5\sum_{h=2}^{2H}\mathfrak{u}_h\mathbf{M}^h(t)\\&\quad+\mathfrak{b}\mathcal{G}\big(\mathbf{N}(t),0\big)-\mathfrak{b}\mathcal{G}\big(\mathbf{N}(t),\mathbf{M}(t)\big).\end{aligned}$$

To eliminate the term associated with $\mathbf{M}(t)$, we set

$$f_\beta(t)=-\ln\mathbf{M}(t)+\frac{\mathfrak{b}\varpi}{\mathfrak{m}_{10}\mathfrak{m}_{11}}\Big(\ln\mathbf{U}(t)-\ln\mathbf{N}(t)\Big)+\beta\mathbf{M}(t),$$

where the positive constant $\beta$ verifies

$$\beta\mathcal{Q}_1\ge\left(\mathfrak{m}_{20}\mathfrak{m}_{21}+\frac{\mathfrak{b}^2\varpi^2}{\mathfrak{m}_{10}\mathfrak{m}_{11}}\right).$$

Then, we have

$$\begin{aligned}\mathcal{L}f_\beta(t)&\le\overbrace{-\mathfrak{b}\int_{\mathbb{R}_+}\mathcal{G}(y,0)\pi^{\mathbf{U}}(\mathrm{d}y)+\mathcal{Q}_1+0.5\mathfrak{m}_{20}^2}^{=-\mathfrak{R}_\star^\Sigma}\\&\quad+\mathfrak{b}\left(\int_{\mathbb{R}_+}\mathcal{G}(y,0)\pi^{\mathbf{U}}(\mathrm{d}y)-\mathcal{G}\big(\mathbf{U}(t),0\big)\right)\\&\quad+\beta\mathfrak{b}\mathcal{G}\big(\mathbf{N}(t),\mathbf{M}(t)\big)\mathbf{M}(t)+0.5\sum_{h=2}^{2H}\mathfrak{u}_h\mathbf{M}^h(t)+\mathfrak{b}\mathcal{G}\big(\mathbf{N}(t),0\big)\\&\quad-\mathfrak{b}\mathcal{G}\big(\mathbf{N}(t),\mathbf{M}(t)\big).\end{aligned}$$

In the same vein, we apply the differential operator $\mathcal{L}$ on the function $\kappa^{-1}\big(1+\mathbf{N}(t)\big)^\kappa+\kappa^{-1}\mathbf{M}^\kappa(t)$, $\kappa\in(0,1)$, then

$$\begin{aligned}&\mathcal{L}\Big(\kappa^{-1}\big(1+\mathbf{N}(t)\big)^\kappa+\kappa^{-1}\mathbf{M}^\kappa(t)\Big)\\&=\big(1+\mathbf{N}(t)\big)^{\kappa-1}\Big(\mathcal{Q}_0N_\star-\mathcal{Q}_0\mathbf{N}(t)-\mathfrak{b}\mathcal{G}\big(\mathbf{N}(t),\mathbf{M}(t)\big)\mathbf{M}(t)\Big)\\&\quad+0.5(\kappa-1)\big(1+\mathbf{N}(t)\big)^{\kappa-2}\left(\sum_{h=0}^{H}\mathfrak{m}_{1h}\mathbf{N}^{h+1}(t)\right)^2\\&\quad+\mathbf{M}^{\kappa-1}(t)\Big(\mathfrak{b}\mathcal{G}\big(\mathbf{N}(t),\mathbf{M}(t)\big)\mathbf{M}(t)-\mathcal{Q}_1\mathbf{M}(t)\Big)\\&\quad+0.5(\kappa-1)\mathbf{M}^{\kappa-2}(t)\left(\sum_{h=0}^{H}\mathfrak{m}_{2h}\mathbf{M}^{h+1}(t)\right)^2.\end{aligned}$$

Accordingly, we derive that

$$\begin{aligned}&\mathcal{L}\Big(\kappa^{-1}\big(1+\mathbf{N}(t)\big)^\kappa+\kappa^{-1}\mathbf{M}^\kappa(t)\Big)\\&\le\mathcal{Q}_0N_\star-0.5(1-\kappa)\mathfrak{m}_{11}^2\mathbf{N}^{\kappa+2}(t)+\mathfrak{b}\varpi\mathbf{N}(t)\mathbf{M}^\kappa(t)\\&\quad-\Big(\mathcal{Q}_1+0.5(1-\kappa)\mathfrak{m}_{20}^2\Big)\mathbf{M}^\kappa(t)\\&\quad+(1-\kappa)\mathfrak{m}_{20}\mathfrak{m}_{21}\mathbf{M}^{\kappa+1}(t)-0.5(1-\kappa)\mathfrak{m}_{21}^2\mathbf{M}^{\kappa+2}(t)\\&\quad-0.5(1-\kappa)\sum_{h=2}^{2H}\mathfrak{u}_h\mathbf{M}^{h+\kappa}(t)\\&\le\mathcal{Q}_0N_\star-0.5(1-\kappa)\mathfrak{m}_{11}^2\mathbf{N}^{\kappa+2}(t)+\mathfrak{b}\varpi(\kappa+1)^{-1}\mathbf{N}^{\kappa+1}(t)\\&\quad+\mathfrak{b}\varpi\kappa(\kappa+1)^{-1}\mathbf{M}^{\kappa+1}(t)\\&\quad-0.5(1-\kappa)\mathfrak{m}_{21}^2\mathbf{M}^{\kappa+2}(t)-0.5(1-\kappa)\sum_{h=2}^{2H}\mathfrak{u}_h\mathbf{M}^{h+\kappa}(t).\end{aligned}$$

Now, we define a new function $f_{\beta,\kappa}$ as follows:

$$f_{\beta,\kappa}(\mathbf{N},\mathbf{M})=Sf_\beta+\kappa^{-1}\big(1+\mathbf{N}\big)^\kappa+\kappa^{-1}\mathbf{M}^\kappa,$$

where $S>0$ satisfies that $-S\mathfrak{R}_\star^\Sigma+\mathcal{D}+2\le0$ and $\mathcal{D}$ is given by

$$\begin{aligned}\mathcal{D}=\max\Bigg\{\sup_{(\mathbf{N},\mathbf{M})\in\mathbb{R}_{+,\star}^2}\Bigg\{&\mathcal{Q}_0N_\star+\mathfrak{b}\varpi(\kappa+1)^{-1}\mathbf{N}^{\kappa+1}(t)\\&-0.25(1-\kappa)\mathfrak{m}_{11}^2\mathbf{N}^{\kappa+2}(t)+\mathfrak{b}\varpi\kappa(\kappa+1)^{-1}\mathbf{M}^{\kappa+1}(t)\\&-0.25(1-\kappa)\mathfrak{m}_{21}^2\mathbf{M}^{\kappa+2}(t)+0.5\sum_{h=2}^{2H}\mathfrak{u}_h\mathbf{M}^h(t)\\&-0.5(1-\kappa)\sum_{h=2}^{2H}\mathfrak{u}_h\mathbf{M}^{h+\kappa}(t)\Bigg\},1\Bigg\}.\end{aligned}$$

Clearly, the function $f_{\beta,\kappa}$ reaches its minimum value at a point $(\mathbf{N}^\ell,\mathbf{M}^\ell)$. For this reason, we will consider a new non-negative function defined as follows:

$$f_{\beta,\kappa}^\Sigma(\mathbf{N},\mathbf{M})=Sf_\beta+\kappa^{-1}\big(1+\mathbf{N}\big)^\kappa+\kappa^{-1}\mathbf{M}^\kappa-f_{\beta,\kappa}(\mathbf{N}^\ell,\mathbf{M}^\ell).$$

From the above calculation, we obtain

$$\begin{aligned}\mathcal{L}f_{\beta,\kappa}^\Sigma(t)&\le-S\mathfrak{R}_\star^\Sigma+S\beta\mathfrak{b}\varpi\mathbf{N}(t)\mathbf{M}(t)+\mathfrak{b}S\Big(\mathcal{G}\big(\mathbf{N}(t),0\big)-\mathcal{G}\big(\mathbf{N}(t),\mathbf{M}(t)\big)\Big)\\&\quad+0.5S\sum_{h=2}^{2H}\mathfrak{u}_h\mathbf{M}^h(t)\end{aligned}$$

$$
\begin{aligned}
&+\mathcal{Q}_0 N_\star - 0.5(1-\kappa)\mathfrak{m}_{11}^2\mathbf{N}^{\kappa+2}(t) + \mathfrak{b}\varpi(\kappa+1)^{-1}\mathbf{N}^{\kappa+1}(t)\\
&+\mathfrak{b}\varpi\kappa(\kappa+1)^{-1}\mathbf{M}^{\kappa+1}(t)\\
&-0.5(1-\kappa)\mathfrak{m}_{21}^2\mathbf{M}^{\kappa+2}(t) - 0.5(1-\kappa)\sum_{h=2}^{2H}\mathfrak{u}_h\mathbf{M}^{h+\kappa}(t)\\
&+\mathfrak{b}S\left(\int_{\mathbb{R}_+}\mathcal{G}(y,0)\pi^{\mathbf{U}}(\mathrm{d}y) - \mathcal{G}\big(\mathbf{U}(t),0\big)\right)\\
&= g\big(\mathbf{N}(t),\mathbf{M}(t)\big) + \mathfrak{b}S\left(\int_{\mathbb{R}_+}\mathcal{G}(y,0)\pi^{\mathbf{U}}(\mathrm{d}y) - \mathcal{G}\big(\mathbf{U}(t),0\big)\right).
\end{aligned}
$$

To continue our analysis, we need to define the following five sets:

$$
\begin{aligned}
\mathcal{A}_{a,a_\dagger} &= \Big\{\big(\mathbf{N}(t),\mathbf{M}(t)\big)\in\mathbb{R}_+^{2,\star}|\ \ a\le\mathbf{N}(t)\le a^{-1},\ \ a_\dagger\le\mathbf{M}(t)\le a_\dagger^{-1}\Big\},\\
\mathcal{A}_{a,1} &= \Big\{\big(\mathbf{N}(t),\mathbf{M}(t)\big)\in\mathbb{R}_+^{2,\star}|\ \ 0<\mathbf{N}(t)<a\Big\},\\
\mathcal{A}_{a_\dagger,2} &= \Big\{\big(\mathbf{N}(t),\mathbf{M}(t)\big)\in\mathbb{R}_+^{2,\star}|\ \ 0<\mathbf{M}(t)<a_\dagger\Big\},\\
\mathcal{A}_{a,3} &= \Big\{\big(\mathbf{N}(t),\mathbf{M}(t)\big)\in\mathbb{R}_+^{2,\star}|\ \ \mathbf{N}(t)>a^{-1}\Big\},\\
\mathcal{A}_{a_\dagger,4} &= \Big\{\big(\mathbf{N}(t),\mathbf{M}(t)\big)\in\mathbb{R}_+^{2,\star}|\ \ \mathbf{M}(t)>a_\dagger^{-1}\Big\}.
\end{aligned}
$$

Here, $\mathbb{R}_+^{2,\star}=\{(x,y):\ x>0,y>0\}$, $a_\dagger=\min\{a_\circ,a\}$, where $a_\circ>0$ verifies (2.11), and $a>0$ is chosen carefully such that

$$
S\beta\mathfrak{b}\varpi a + \mathfrak{b}S\varpi a + \frac{\kappa S\beta\mathfrak{b}\varpi a}{\kappa+2}\left(\frac{2S\beta\mathfrak{b}\varpi a}{0.25(\kappa+2)(1-\kappa)\mathfrak{m}_{21}^2}\right)^{2\kappa^{-1}} - 1\le 0, \tag{2.6}
$$

$$
S\beta\mathfrak{b}\varpi a + \frac{\kappa S\beta\mathfrak{b}\varpi a}{\kappa+2}\left(\frac{2S\beta\mathfrak{b}\varpi a}{0.25(\kappa+2)(1-\kappa)\mathfrak{m}_{11}^2}\right)^{2\kappa^{-1}} - 1 < 0, \tag{2.7}
$$

$$
-S\mathfrak{R}_\star^\Sigma + \mathfrak{Z} - 0.25(1-\kappa)\mathfrak{m}_{11}^2 a^{-\kappa-2} + 1\le 0, \tag{2.8}
$$

$$
-S\mathfrak{R}_\star^\Sigma + \mathfrak{Z} - 0.25(1-\kappa)\mathfrak{m}_{21}^2 a^{-\kappa-2} + 1\le 0, \tag{2.9}
$$

where

$$
\begin{aligned}
\mathfrak{Z} = \sup_{(\mathbf{N},\mathbf{M})\in\mathbb{R}_+^{2,\star}}\Big\{&0.5S\beta\mathfrak{b}\varpi\mathbf{N}^2(t) + 0.5S\beta\mathfrak{b}\varpi\mathbf{M}^2(t) + S\mathfrak{b}\varpi\mathbf{N}(t)\\
&+\mathcal{Q}_0N_\star + \mathfrak{b}\varpi(\kappa+1)^{-1}\mathbf{N}^{\kappa+1}(t)\\
&+\mathfrak{b}\varpi\kappa(\kappa+1)^{-1}\mathbf{M}^{\kappa+1}(t) - 0.25(1-\kappa)\mathfrak{m}_{11}^2\mathbf{N}^{\kappa+2}(t)\\
&-0.25(1-\kappa)\mathfrak{m}_{21}^2\mathbf{M}^{\kappa+2}(t)\\
&+0.5S\sum_{h=2}^{2H}\mathfrak{u}_h\mathbf{M}^h(t) - 0.5(1-\kappa)\sum_{h=2}^{2H}\mathfrak{u}_h\mathbf{M}^{h+\kappa}(t)\Big\}.
\end{aligned}
$$

Plainly, $\mathcal{A}_{a,a_\dagger}^c=\mathbb{R}_+^{2,\star}\setminus\mathcal{A}_{a,a_\dagger}=\mathcal{A}_{a,1}\cup\mathcal{A}_{a_\dagger,2}\cup\mathcal{A}_{a,3}\cup\mathcal{A}_{a_\dagger,4}$. In the following, we will verify that

$$
1+g\big(\mathbf{N}(t),\mathbf{M}(t)\big)\le 0, \tag{2.10}
$$

for any $\big(\mathbf{N}(t),\mathbf{M}(t)\big)\in\mathcal{A}_{a,a_\dagger}^c$ which is equivalent to showing it on $\mathcal{A}_{a,1}$, $\mathcal{A}_{a_\dagger,2}$, $\mathcal{A}_{a,3}$ and $\mathcal{A}_{a_\dagger,4}$, respectively. For this reason, we have the following situations:

1 **Situation 1**: assume that $\big(\mathbf{N}(t),\mathbf{M}(t)\big)\in\mathcal{A}_{a,1}$. From (2.6), we obtain

$$
\begin{aligned}
g\big(\mathbf{N}(t),\mathbf{M}(t)\big) &\le -S\mathfrak{R}_\star^\Sigma + S\beta\mathfrak{b}\varpi a + \mathfrak{b}S\varpi a + S\beta\mathfrak{b}\varpi a\mathbf{M}^2(t)\\
&\quad - 0.25(1-\kappa)\mathfrak{m}_{11}^2\mathbf{N}^{\kappa+2}(t) + S0.5\sum_{h=2}^{2H}\mathfrak{u}_h\mathbf{M}^h(t)\\
&\quad + \mathcal{Q}_0N_\star + \mathfrak{b}\varpi(\kappa+1)^{-1}\mathbf{N}(t)^{\kappa+1} + \mathfrak{b}\varpi\kappa(\kappa+1)^{-1}\mathbf{M}^{\kappa+1}(t)\\
&\quad - 0.25(1-\kappa)\mathfrak{m}_{21}^2\mathbf{M}^{\kappa+2}(t)\\
&\quad - 0.25(1-\kappa)\mathfrak{m}_{21}^2\mathbf{M}^{\kappa+2}(t) - 0.5(1-\kappa)\sum_{h=2}^{2H}\mathfrak{u}_h\mathbf{M}^{h+\kappa}(t)\\
&\le -S\mathfrak{R}_\star^\Sigma + \mathcal{D} + S\beta\mathfrak{b}\varpi a + \mathfrak{b}S\varpi a\\
&\quad + \frac{\kappa S\beta\mathfrak{b}\varpi a}{\kappa+2}\left(\frac{2S\beta\mathfrak{b}\varpi a}{0.25(\kappa+2)(1-\kappa)\mathfrak{m}_{21}^2}\right)^{2\kappa^{-1}}\\
&\le -1.
\end{aligned}
$$

2 **Situation 2**: here, we use the uniform continuity at $\mathbf{M}=0$ of the function $\mathcal{G}\big(\mathbf{N}(t),\mathbf{M}(t)\big)$. By assumption $\mathbf{A_a}$, $\exists a_\circ>0$ such that as $0<\mathbf{M}\le a_\circ$,

$$
\begin{aligned}
&S\beta\mathfrak{b}\varpi a + \frac{\kappa S\beta\mathfrak{b}\varpi a}{\kappa+2}\left(\frac{2S\beta\mathfrak{b}\varpi a}{0.25(\kappa+2)(1-\kappa)\mathfrak{m}_{11}^2}\right)^{2\kappa^{-1}}\\
&\quad + \mathfrak{b}S\Big(\mathcal{G}\big(\mathbf{N}(t),0\big) - \mathcal{G}\big(\mathbf{N}(t),\mathbf{M}(t)\big)\Big) < 1.
\end{aligned} \tag{2.11}
$$

Consequently, if $\mathbf{M}<a_\dagger=\min\{a_\circ,a\}$, we get from (2.7) that

$$
\begin{aligned}
&g\big(\mathbf{N}(t),\mathbf{M}(t)\big)\\
&\le -S\mathfrak{R}_\star^\Sigma + S\beta\mathfrak{b}\varpi a + S\beta\mathfrak{b}\varpi a\mathbf{N}^2(t) - 0.25(1-\kappa)\mathfrak{m}_{11}^2\mathbf{N}^{\kappa+2}(t)\\
&\quad + 0.5S\sum_{h=2}^{2H}\mathfrak{u}_h\mathbf{M}^h(t) + \mathcal{Q}_0N_\star\\
&\quad + \mathfrak{b}S\Big(\mathcal{G}\big(\mathbf{N}(t),0\big) - \mathcal{G}\big(\mathbf{N}(t),\mathbf{M}(t)\big)\Big) + \mathfrak{b}\varpi(\kappa+1)^{-1}\mathbf{N}(t)^{\kappa+1}\\
&\quad + \mathfrak{b}\varpi\kappa(\kappa+1)^{-1}\mathbf{M}^{\kappa+1}(t)\\
&\quad - 0.25(1-\kappa)\mathfrak{m}_{21}^2\mathbf{M}^{\kappa+2}(t)\\
&\quad - 0.5(1-\kappa)\sum_{h=2}^{2H}\mathfrak{u}_h\mathbf{M}^{h+\kappa}(t)\\
&\le -S\mathfrak{R}_\star^\Sigma + \mathcal{D} + S\beta\mathfrak{b}\varpi a + \frac{\kappa S\beta\mathfrak{b}\varpi a}{\kappa+2}\left(\frac{2S\beta\mathfrak{b}\varpi a}{0.25(\kappa+2)(1-\kappa)\mathfrak{m}_{11}^2}\right)^{2\kappa^{-1}}\\
&\quad + \mathfrak{b}S\Big(\mathcal{G}\big(\mathbf{N}(t),0\big) - \mathcal{G}\big(\mathbf{N}(t),\mathbf{M}(t)\big)\Big)\\
&\le -1.
\end{aligned}
$$

3 **Situation 3**: assume that $\big(\mathbf{N}(t),\mathbf{M}(t)\big)\in\mathcal{A}_{a,3}$. From (2.8), we have

$$
\begin{aligned}
g\big(\mathbf{N}(t),\mathbf{M}(t)\big) &\le -S\mathfrak{R}_\star^\Sigma - 0.25(1-\kappa)\mathfrak{m}_{11}^2\mathbf{N}^{\kappa+2}(t) + 0.5S\beta\mathfrak{b}\varpi\mathbf{N}^2(t)\\
&\quad + 0.5S\beta\mathfrak{b}\varpi\mathbf{M}^2(t) + S\mathfrak{b}\varpi\mathbf{N}(t)\\
&\quad + \mathcal{Q}_0N_\star + \mathfrak{b}\varpi(\kappa+1)^{-1}\mathbf{N}(t)^{\kappa+1} + \mathfrak{b}\varpi\kappa(\kappa+1)^{-1}\mathbf{M}^{\kappa+1}(t)\\
&\quad - 0.25(1-\kappa)\mathfrak{m}_{11}^2\mathbf{N}^{\kappa+2}(t)\\
&\quad - 0.25(1-\kappa)\mathfrak{m}_{21}^2\mathbf{M}^{\kappa+2}(t) + 0.5S\sum_{h=2}^{2H}\mathfrak{u}_h\mathbf{M}^h(t)\\
&\quad - 0.5(1-\kappa)\sum_{h=2}^{2H}\mathfrak{u}_h\mathbf{M}^{h+\kappa}(t)\\
&\le -S\mathfrak{R}_\star^\Sigma + \mathfrak{Z} - 0.25(1-\kappa)\mathfrak{m}_{11}^2 a^{-\kappa-2}\\
&\le -1.
\end{aligned}
$$

4 **Situation 4**: assume that $\big(\mathbf{N}(t),\mathbf{M}(t)\big)\in\mathcal{A}_{a_\dagger,4}$. From (2.9), we get

$$
\begin{aligned}
g\big(\mathbf{N}(t),\mathbf{M}(t)\big) &\le -S\mathfrak{R}_\star^\Sigma - 0.25(1-\kappa)\mathfrak{m}_{21}^2\mathbf{M}^{\kappa+2}(t) + 0.5S\beta\mathfrak{b}\varpi\mathbf{N}^2(t)\\
&\quad + 0.5S\beta\mathfrak{b}\varpi\mathbf{M}^2(t) + S\mathfrak{b}\varpi\mathbf{N}(t)\\
&\quad + \mathcal{Q}_0N_\star + \mathfrak{b}\varpi(\kappa+1)^{-1}\mathbf{N}(t)^{\kappa+1}\\
&\quad + \mathfrak{b}\varpi\kappa(\kappa+1)^{-1}\mathbf{M}^{\kappa+1}(t) - 0.25(1-\kappa)\mathfrak{m}_{11}^2\mathbf{N}^{\kappa+2}(t)\\
&\quad - 0.25(1-\kappa)\mathfrak{m}_{21}^2\mathbf{M}^{\kappa+2}(t) + 0.5S\sum_{h=2}^{2H}\mathfrak{u}_h\mathbf{M}^h(t)\\
&\quad - 0.5(1-\kappa)\sum_{h=2}^{2H}\mathfrak{u}_h\mathbf{M}^{h+\kappa}(t)\\
&\le -S\mathfrak{R}_\star^\Sigma + \mathfrak{Z} - 0.25(1-\kappa)\mathfrak{m}_{21}^2 a^{-\kappa-2}\\
&\le -1.
\end{aligned}
$$

**Table 3**
Some values used in the traditional wastewater process with a fully mixed flow reactor.

| Parameters | Standard domain | Units | Scenario 1 | Scenario 2 |
|---|---|---|---|---|
| $\theta$: Hydraulic retention time | 0.5–7.5 | day | 1.97 | 2.95 |
| $\mathfrak{b}$: Constant growth of bacteria | 2–10 | mg of cells × day | 8 | 8 |
| $\mathfrak{K}_{\mathbf{N}}$: Saturation constant of N | 25–100 | mg of cells × day/$\ell$ | 60 | 60 |
| $\mathfrak{K}_{\mathbf{M}}$: Saturation constant of M | 25–100 | mg of cells × day/$\ell$ | 60 | 60 |
| $Q_d$: Death ratio of M | 0.025–0.075 | 1/day | 0.06 | 0.06 |
| $R_c$: Recycle percentage | 25%–75% | – | 50% | 50% |
| $N_\star$: Input concentration | – | mg of cells × day/$\ell$ | 15 | 15 |

In summary, the assertion (2.10) is verified. On the other hand, we can easily show that $\exists \mathcal{O} > 0$ such that $g(\mathbf{N},\mathbf{M}) \leq \mathcal{O}$, for all $(\mathbf{N},\mathbf{M}) \in \mathbb{R}^{2,\star}_+$. Accordingly, we get

$$\begin{aligned}
&\int_0^t \mathbb{E}\big(g(\mathbf{N}(\tau),\mathbf{M}(\tau))\big)\mathrm{d}\tau \\
&\quad + S\varpi\mathbb{E}\bigg(\int_0^t\int_0^\infty \mathcal{G}(y,0)\pi^{\mathbf{U}}(\mathrm{d}y)\mathrm{d}\tau - \int_0^t \mathcal{G}(\mathbf{U}(\tau),0)\mathrm{d}\tau\bigg) \\
&\geq \int_0^t \mathbb{E}\Big(\mathcal{L}f^{\Sigma}_{\beta,\kappa}(\mathbf{N}(\tau),\mathbf{M}(\tau))\Big)\mathrm{d}\tau \\
&= \mathbb{E}\Big(f^{\Sigma}_{\beta,\kappa}(\mathbf{N}(t),\mathbf{M}(t))\Big) - \mathbb{E}\Big(f^{\Sigma}_{\beta,\kappa}(\mathbf{N}(0),\mathbf{M}(0))\Big) \\
&\geq -\mathbb{E}\Big(f^{\Sigma}_{\beta,\kappa}(\mathbf{N}(0),\mathbf{M}(0))\Big).
\end{aligned}$$

By using the ergodic property of $\mathbf{U}(t)$, we conclude that

$$\begin{aligned}
0 &\leq \liminf_{t\to\infty} t^{-1}\int_0^t \bigg(\mathbb{E}g(\mathbf{N}(\tau),\mathbf{M}(\tau))\mathbb{1}_{\{(\mathbf{N}(\tau),\mathbf{M}(\tau))\in\mathcal{A}^c_{a,a_\dagger}\}} \\
&\quad + \mathbb{E}g(\mathbf{N}(\tau),\mathbf{M}(\tau))\mathbb{1}_{\{(\mathbf{N}(\tau),\mathbf{M}(\tau))\in\mathcal{A}_{a,a_\dagger}\}}\bigg)\mathrm{d}\tau \\
&\leq \liminf_{t\to\infty} t^{-1}\int_0^t \Big(-\mathbb{P}\big((\mathbf{N}(\tau),\mathbf{M}(\tau))\in\mathcal{A}^c_{a,a_\dagger}\big) \\
&\quad + \mathcal{O}\mathbb{P}\big((\mathbf{N}(\tau),\mathbf{M}(\tau))\in\mathcal{A}_{a,a_\dagger}\big)\Big)\mathrm{d}\tau \\
&= -1 + (1+\mathcal{O})\liminf_{t\to\infty} t^{-1}\int_0^t \mathbb{P}\big((\mathbf{N}(\tau),\mathbf{M}(\tau))\in\mathcal{A}_{a,a_\dagger}\big)\mathrm{d}\tau.
\end{aligned}$$

Consequently

$$\liminf_{t\to\infty} t^{-1}\int_0^t \mathbb{P}\Big(\big(\mathbf{N}(\tau),\mathbf{M}(\tau)\big)\in\mathcal{A}_{a,a_\dagger}\Big)\mathrm{d}\tau \geq (1+\mathcal{O})^{-1} > 0.$$

Hence

$$\liminf_{t\to\infty} t^{-1}\int_0^t \mathbb{P}\Big(\big(\mathbf{N}(0),\mathbf{M}(0)\big);\tau,\mathcal{A}_{a,a_\dagger}\Big)\mathrm{d}\tau > 0, \qquad \forall\big(\mathbf{N}(0),\mathbf{M}(0)\big)\in\mathbb{R}^{2,\star}_+.$$

Identical to the demonstration of (Lemma 3.2., [68]) and the mutually limited possibilities lemma [69], we establish the existence, uniqueness and ergodicity of a single invariant distribution $\pi^{\Sigma}$ for the perturbed model (1.3). □

## Numerical experiment: Industrial wastewater treatment

This section is devoted to numerically verifying the above-mentioned theoretical results. We aim to make sure that $\mathcal{R}^{\Sigma}_{\circ}$ is the sharp sill of the model (1.3). So, we present three situations of system (1.3), and in each case, we explore the complex long-run behavior of the bacteria. As an instance of the function $\mathcal{G}$, we use the Beddington–DeAngelis interference function introduced in Table 1. We apply the Euler–Maruyama method to discretize the disturbed system (1.3). By using the software Matlab2015b and the parameter values listed in Table 3 (taken from [12]), we deal with two scenarios of wastewater operation under heavy fluctuations.

**Remark 3.1.** The threshold of our model with Beddington–DeAngelis interference function is expressed by

$$\begin{aligned}
\mathfrak{R}^{\Sigma}_{\star} &= \mathfrak{b}\int_{\mathbb{R}_+}\mathcal{G}(y,0)\pi^{\mathbf{U}}(\mathrm{d}y) - \mathcal{Q}_1 - 0.5\mathfrak{m}^2_{20} \\
&= \lim_{T\to\infty} T^{-1}\int_0^T \frac{\mathfrak{b}\mathbf{U}(\tau)}{1+\mathfrak{K}_{\mathbf{N}}\mathbf{U}(\tau)}\mathrm{d}\tau - \mathcal{Q}_1 - 0.5\mathfrak{m}^2_{20}.
\end{aligned}$$

The probability density function $\pi^{\mathbf{U}}$ obeys a Fokker–Planck equation, which is easy to approximate it through Monte Carlo simulations. Via ergodic property, we can also estimate this quantity

$$\lim_{T\to\infty} T^{-1}\int_0^T \frac{\mathfrak{b}\mathbf{U}(\tau)}{1+\mathfrak{K}_{\mathbf{N}}\mathbf{U}(\tau)}\mathrm{d}\tau,$$

for a large time $T$. This last technique is the one that we will use in our simulations. Since the equation of $\mathbf{U}$ is disturbed by polynomial fluctuations, said limit will be modified according to the magnitude of the intensity and, consequently, the threshold will also be changed.

*Linear perturbation case ($H = 0$)*

In this case, we numerically study the model treated in [18] which takes the following system:

$$\begin{cases}
\mathrm{d}\mathbf{N}(t) = \Big(\frac{1}{\theta}\big(N_\star - \mathbf{N}(t)\big) - \frac{\mathfrak{b}\mathbf{N}(t)\mathbf{M}(t)}{1+\mathfrak{K}_{\mathbf{N}}\mathbf{N}(t)+\mathfrak{K}_{\mathbf{M}}\mathbf{M}(t)}\Big)\mathrm{d}t \\
\qquad\qquad +0.1\mathbf{N}(t)\mathrm{d}\mathbf{W}_1(t), \\
\mathrm{d}\mathbf{M}(t) = \Big(\frac{\mathfrak{b}\mathbf{N}(t)\mathbf{M}(t)}{1+\mathfrak{K}_{\mathbf{N}}\mathbf{N}(t)+\mathfrak{K}_{\mathbf{M}}\mathbf{M}(t)} - \Big(Q_d + \frac{1+R_c}{\theta}\Big)\mathbf{M}(t)\Big)\mathrm{d}t \\
\qquad\qquad +0.3\mathbf{M}(t)\mathrm{d}\mathbf{W}_2(t), \\
\mathbf{N}(0) = 10, \quad \mathbf{M}(0) = 4.5,
\end{cases} \tag{3.1}$$

associated with the following auxiliary process:

$$\mathrm{d}\mathbf{U}(t) = \Big(\frac{1}{\theta}\big(N_\star - \mathbf{U}(t)\big)\Big)\mathrm{d}t + 0.1\mathbf{U}(t)\mathrm{d}\mathbf{W}_1(t), \qquad \mathbf{U}(0) = 10.$$

Practically, we have the following two scenarios.

*Scenario 1: Disappearance of bacteria*

By selecting parameters values from Table 3 (Scenario 1) and choosing a sufficiently large number $T > 0$, we obtain

$$\begin{aligned}
\mathfrak{R}^{\Sigma}_{\star} &= \mathfrak{b}\int_{\mathbb{R}_+}\mathcal{G}(y,0)\pi^{\mathbf{U}}(\mathrm{d}y) - \mathcal{Q}_1 - 0.5\mathfrak{m}^2_{20} \\
&= \lim_{T\to\infty} T^{-1}\int_0^T \frac{\mathfrak{b}\mathbf{U}(\tau)}{1+\mathfrak{K}_{\mathbf{N}}\mathbf{U}(\tau)}\mathrm{d}\tau - \mathcal{Q}_1 - 0.5\mathfrak{m}^2_{20} = -0.0028 < 0.
\end{aligned}$$

It follows from Theorem 2.1 that the bacteria $\mathbf{M}$ in wastewater chemostat process go to extinction with probability one and the substrate $\mathbf{N}$ persists. Fig. 2 is the corresponding numerical simulation diagram.

*Scenario 2: Persistence of bacteria*

Now, we choose parameters values from Table 3 (Scenario 2) to move from the case of extinction to the case of continuation. Then

$$\begin{aligned}
\mathfrak{R}^{\Sigma}_{\star} &= \mathfrak{b}\int_{\mathbb{R}_+}\mathcal{G}(y,0)\pi^{\mathbf{U}}(\mathrm{d}y) - \mathcal{Q}_1 - 0.5\mathfrak{m}^2_{20} \\
&= \lim_{T\to\infty} T^{-1}\int_0^T \frac{\mathfrak{b}\mathbf{U}(\tau)}{1+\mathfrak{K}_{\mathbf{N}}\mathbf{U}(\tau)}\mathrm{d}\tau - \mathcal{Q}_1 - 0.5\mathfrak{m}^2_{20} = 0.0163 > 0.
\end{aligned}$$

Thus, it follows from Theorem 2.2 that there exists a unique ergodic steady distribution of model (3.1). This means that bacteria are still present in the wastewater regulation process and we can collect them constantly. In Fig. 3, we depict the permanence phenomenon by drawing trajectories and sketching the experimental two-dimensional density of $\pi^{\Sigma}(\mathbf{N},\mathbf{M})$.

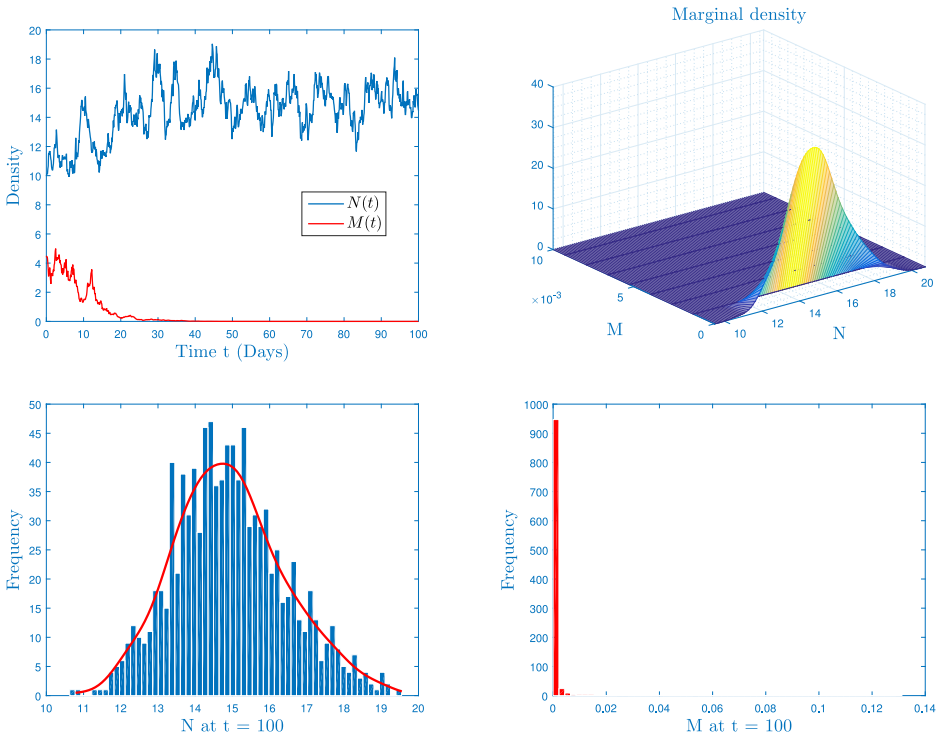


**Fig. 2.** Line I: trajectories of densities $(\mathbf{N}, \mathbf{M})$ and their associated probability density function $\pi^{\Sigma}(\mathbf{N}, \mathbf{M})$. Line II: the projection drawing of $\pi^{\Sigma}$ on different coordinate planes. The deterministic parameters are selected from Table 3 (Scenario 1). For the noise intensities, we select $\mathfrak{m}_{10} = 0.01$ and $\mathfrak{m}_{20} = 0.3$. In this case, $\mathfrak{R}_{\star}^{\Sigma} = -0.0028 < 0$.

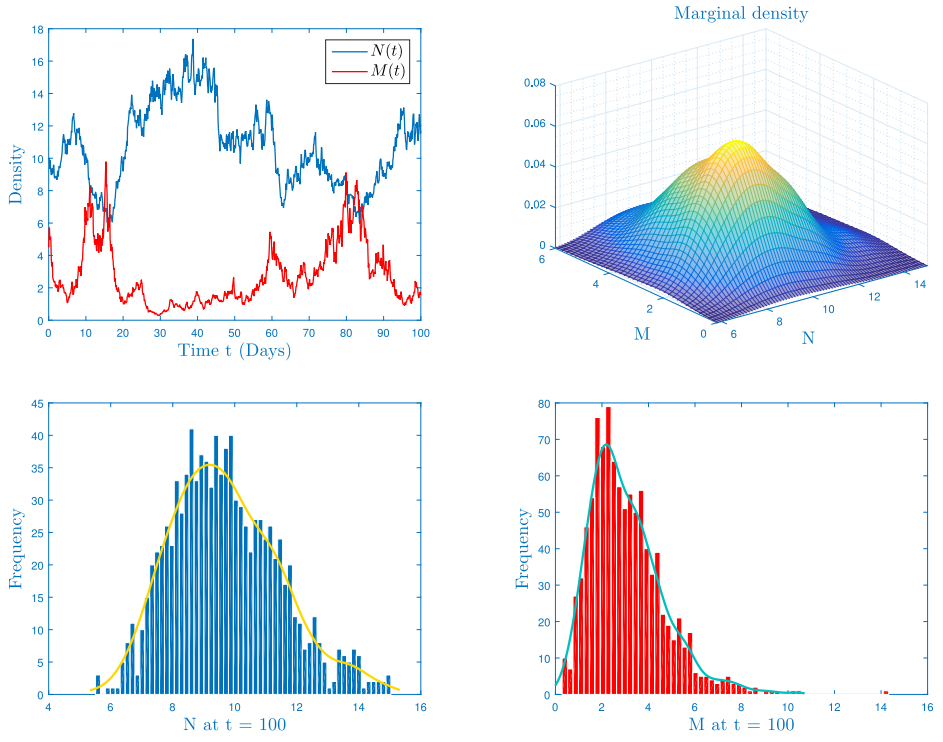


**Fig. 3.** Line I: trajectories of densities $(\mathbf{N}, \mathbf{M})$ and their associated probability density function $\pi^{\Sigma}(\mathbf{N}, \mathbf{M})$. Line II: the projection drawing of $\pi^{\Sigma}$ on different coordinate planes. The deterministic parameters are selected from Table 3 (Scenario 2). For the noise intensities, we select $\mathfrak{m}_{10} = 0.01$ and $\mathfrak{m}_{20} = 0.3$. In this case, $\mathfrak{R}_{\star}^{\Sigma} = 0.0163 > 0$.

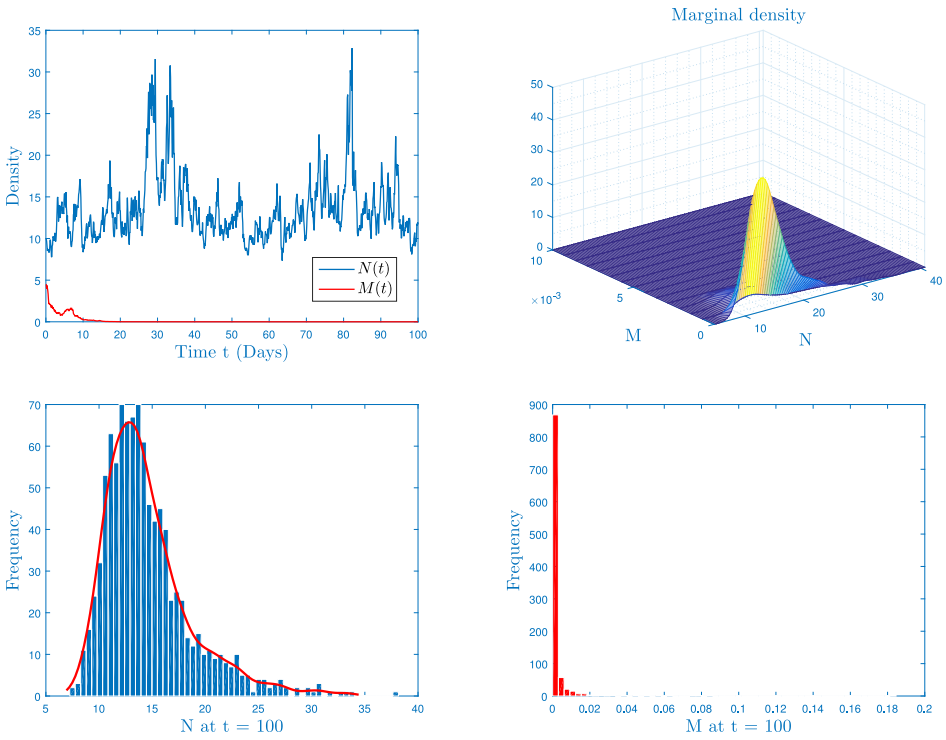


**Fig. 4.** Line I: trajectories of densities $(\mathbf{N},\mathbf{M})$ and their associated probability density function $\pi^{\Sigma}(\mathbf{N},\mathbf{M})$. Line II: the projection drawing of $\pi^{\Sigma}$ on different coordinate planes. The deterministic parameters are selected from Table 3 (Scenario 1). For the noise intensities, we select $\mathfrak{m}_{10} = 0.01$, $\mathfrak{m}_{20} = 0.3$, $\mathfrak{m}_{11} = 0.0122$ and $\mathfrak{m}_{21} = 0.0113$. In this case, $\mathfrak{R}^{\Sigma}_{\star} = -0.0146 < 0$.

*Quadratic perturbation case ($H = 1$)*

In this case, we deal with following probabilistic system:

$$\begin{cases} \mathrm{d}\mathbf{N}(t) = \left(\frac{1}{\theta}\left(N_\star - \mathbf{N}(t)\right) - \frac{\mathfrak{b}\mathbf{N}(t)\mathbf{M}(t)}{1+\mathfrak{K}_{\mathbf{N}}\mathbf{N}(t)+\mathfrak{K}_{\mathbf{M}}\mathbf{M}(t)}\right)\mathrm{d}t \\ \qquad +0.1\mathbf{N}(t)\mathrm{d}\mathbf{W}_1(t) + 0.0122\mathbf{N}^2(t)\mathrm{d}\mathbf{W}_1(t), \\ \mathrm{d}\mathbf{M}(t) = \left(\frac{\mathfrak{b}\mathbf{N}(t)\mathbf{M}(t)}{1+\mathfrak{K}_{\mathbf{N}}\mathbf{N}(t)+\mathfrak{K}_{\mathbf{M}}\mathbf{M}(t)} - \left(Q_d + \frac{1+R_c}{\theta}\right)\mathbf{M}(t)\right)\mathrm{d}t \\ \qquad +0.3\mathbf{M}(t)\mathrm{d}\mathbf{W}_2(t) + 0.0113\mathbf{N}^2(t)\mathrm{d}\mathbf{W}_1(t), \\ \mathbf{N}(0) = 10, \quad \mathbf{M}(0) = 4.5, \end{cases} \tag{3.2}$$

with its corresponding auxiliary process:

$$\mathrm{d}\mathbf{U}(t) = \left(\frac{1}{\theta}\left(N_\star - \mathbf{N}(t)\right)\right)\mathrm{d}t + 0.1\mathbf{U}(t)\mathrm{d}\mathbf{W}_1(t) + 0.0122\mathbf{U}^2(t)\mathrm{d}\mathbf{W}_1(t), \qquad \mathbf{U}(0) = 10.$$

Also, we treat the following two scenarios.

*Scenario 1: Disappearance of bacteria*

By choosing parameters values from Table 3 (Scenario 1) and considering a sufficiently large number $T > 0$, we obtain

$$\begin{aligned} \mathfrak{R}^{\Sigma}_{\star} &= \mathfrak{b}\int_{\mathbb{R}_+} \mathcal{G}(y,0)\pi^{\mathbf{U}}(\mathrm{d}y) - \mathcal{Q}_1 - 0.5\mathfrak{m}_{20}^2 \\ &= \lim_{T\to\infty} T^{-1}\int_0^T \frac{\mathfrak{b}\mathbf{U}(\tau)}{1+\mathfrak{K}_{\mathbf{N}}\mathbf{U}(\tau)}\mathrm{d}\tau - \mathcal{Q}_1 - 0.5\mathfrak{m}_{20}^2 = -0.0146 < 0. \end{aligned}$$

According to Theorem 2.1, we conclude that the bacteria $\mathbf{M}$ in wastewater chemostat process go to extinction with probability one and the substrate $\mathbf{N}$ persists. From Fig. 4, we confirm this theoretical result.

*Scenario 2: Persistence of bacteria*

We select parameters values from Table 3 (Scenario 2) to obtain the continuation of our model. Then

$$\begin{aligned} \mathfrak{R}^{\Sigma}_{\star} &= \mathfrak{b}\int_{\mathbb{R}_+} \mathcal{G}(y,0)\pi^{\mathbf{U}}(\mathrm{d}y) - \mathcal{Q}_1 - 0.5\mathfrak{m}_{20}^2 \\ &= \lim_{T\to\infty} T^{-1}\int_0^T \frac{\mathfrak{b}\mathbf{U}(\tau)}{1+\mathfrak{K}_{\mathbf{N}}\mathbf{U}(\tau)}\mathrm{d}\tau - \mathcal{Q}_1 - 0.5\mathfrak{m}_{20}^2 = 0.0107 > 0. \end{aligned}$$

In accordance with Theorem 2.2, we conclude that there exists a unique ergodic steady distribution of model (3.2). This indicates that bacteria are still present in the wastewater regulation process and we can collect them constantly. In Fig. 5, we illustrate the continuation phenomenon by drawing trajectories and providing the experimental two-dimensional density of $\pi^{\Sigma}(\mathbf{N},\mathbf{M})$.

*Cubic perturbation case ($H = 2$)*

In this part, we numerically prove that $\mathfrak{R}^{\Sigma}_{\circ}$ is the sill of the system (1.3) in the special case of cubic perturbation. So, we firstly introduce this probabilistic model:

$$\begin{cases} \mathrm{d}\mathbf{N}(t) = \left(\frac{1}{\theta}\left(N_\star - \mathbf{N}(t)\right) - \frac{\mathfrak{b}\mathbf{N}(t)\mathbf{M}(t)}{1+\mathfrak{K}_{\mathbf{N}}\mathbf{N}(t)+\mathfrak{K}_{\mathbf{M}}\mathbf{M}(t)}\right)\mathrm{d}t \\ \qquad +0.1\mathbf{N}(t)\mathrm{d}\mathbf{W}_1(t) \\ \qquad +0.0122\mathbf{N}^2(t)\mathrm{d}\mathbf{W}_1(t) + 0.014\mathbf{N}^3(t)\mathrm{d}\mathbf{W}_1(t), \\ \mathrm{d}\mathbf{M}(t) = \left(\frac{\mathfrak{b}\mathbf{N}(t)\mathbf{M}(t)}{1+\mathfrak{K}_{\mathbf{N}}\mathbf{N}(t)+\mathfrak{K}_{\mathbf{M}}\mathbf{M}(t)} - \left(Q_d + \frac{1+R_c}{\theta}\right)\mathbf{M}(t)\right)\mathrm{d}t \\ \qquad +0.3\mathbf{M}(t)\mathrm{d}\mathbf{W}_2(t) \\ \qquad +0.0113\mathbf{M}^2(t)\mathrm{d}\mathbf{W}_2(t) + 0.0135\mathbf{M}^3(t)\mathrm{d}\mathbf{W}_2(t), \\ \mathbf{N}(0) = 10, \quad \mathbf{M}(0) = 4.5, \end{cases} \tag{3.3}$$

with its corresponding auxiliary process:

$$\begin{aligned} \mathrm{d}\mathbf{U}(t) = \left(\frac{1}{\theta}\left(N_\star - \mathbf{U}(t)\right)\right)\mathrm{d}t &+ 0.1\mathbf{U}(t)\mathrm{d}\mathbf{W}_1(t) + 0.0122\mathbf{U}^2(t)\mathrm{d}\mathbf{W}_1(t) \\ &+ 0.014\mathbf{U}^3(t)\mathrm{d}\mathbf{W}_1(t), \qquad \mathbf{U}(0) = 4.5. \end{aligned}$$

Here, we keep the other coefficient values as the above two cases and we deal the following cases.

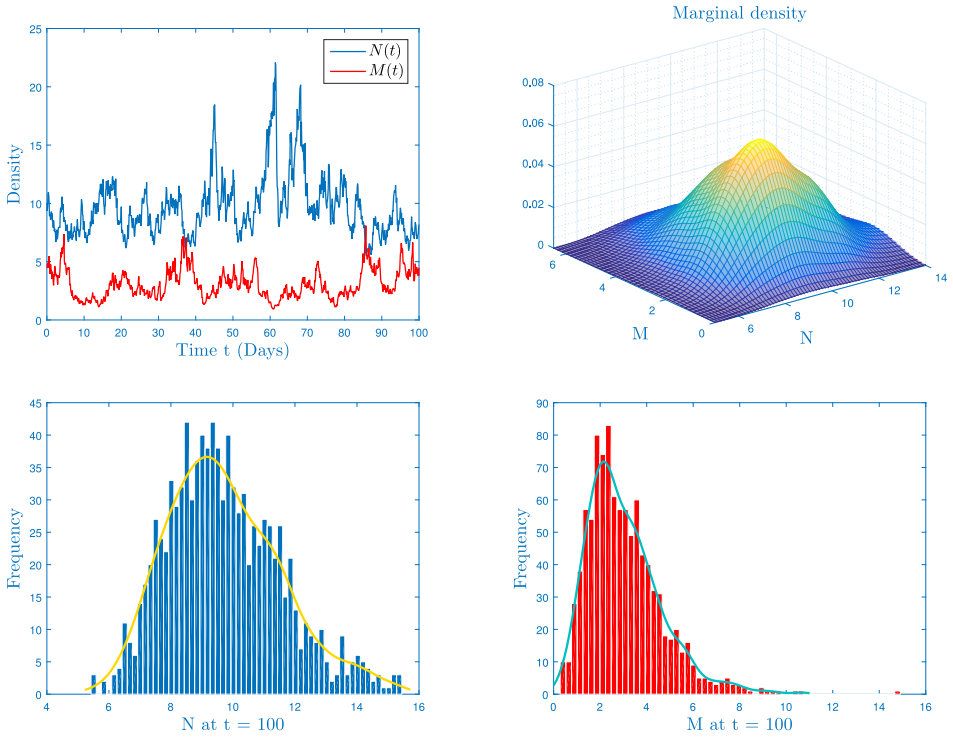


**Fig. 5.** Line I: trajectories of densities $(\mathbf{N},\mathbf{M})$ and their associated probability density function $\pi^{\Sigma}(\mathbf{N},\mathbf{M})$. Line II: the projection drawing of $\pi^{\Sigma}$ on different coordinate planes. The deterministic parameters are selected from Table 3 (Scenario 2). For the noise intensities, we select $\mathfrak{m}_{10} = 0.01$, $\mathfrak{m}_{20} = 0.3$, $\mathfrak{m}_{11} = 0.0122$ and $\mathfrak{m}_{21} = 0.0113$. In this case, $\mathfrak{R}_{\star}^{\Sigma} = 0.0107 > 0$.

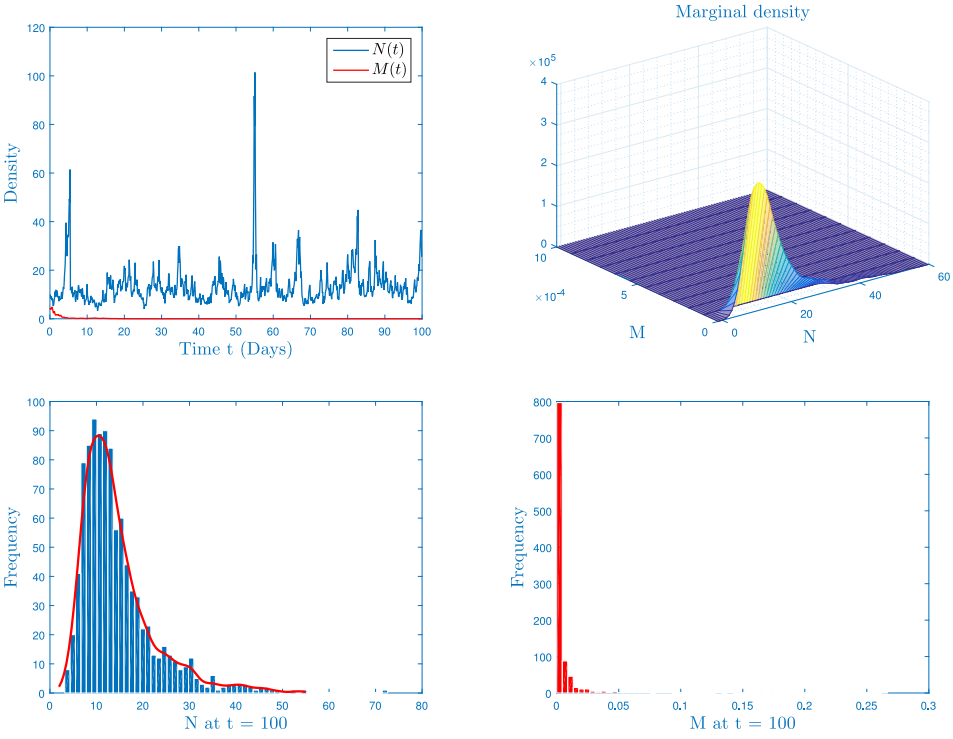


**Fig. 6.** Line I: trajectories of densities $(\mathbf{N},\mathbf{M})$ and their associated probability density function $\pi^{\Sigma}(\mathbf{N},\mathbf{M})$. Line II: the projection drawing of $\pi^{\Sigma}$ on different coordinate planes. The deterministic parameters are selected from Table 3 (Scenario 1). For the noise intensities, we select $\mathfrak{m}_{10} = 0.01$, $\mathfrak{m}_{20} = 0.3$, $\mathfrak{m}_{11} = 0.0122$, $\mathfrak{m}_{21} = 0.0113$, $\mathfrak{m}_{12} = 0.0014$ and $\mathfrak{m}_{22} = 0.0135$. In this case, $\mathfrak{R}_{\star}^{\Sigma} = -0.0511 < 0$.

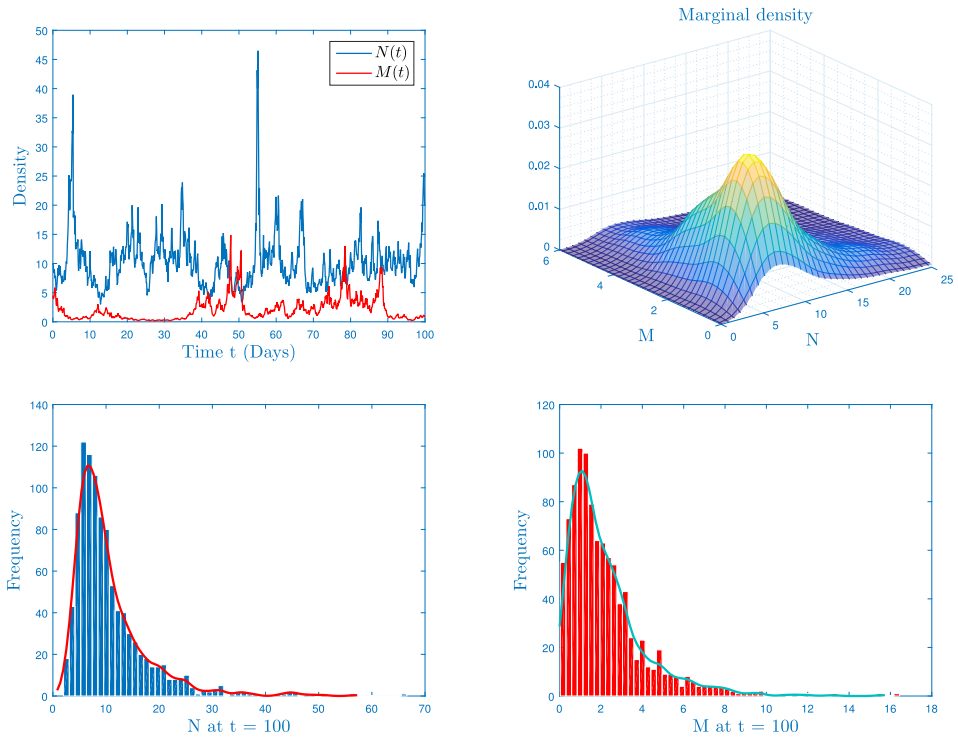


**Fig. 7.** Line I: trajectories of densities $(\mathbf{N},\mathbf{M})$ and their associated probability density function $\pi^{\Sigma}(\mathbf{N},\mathbf{M})$. Line II: the projection drawing of $\pi^{\Sigma}$ on different coordinate planes. The deterministic parameters are selected from Table 3 (Scenario 2). For the noise intensities, we select $\mathfrak{m}_{10} = 0.01$, $\mathfrak{m}_{20} = 0.3$, $\mathfrak{m}_{11} = 0.0122$, $\mathfrak{m}_{21} = 0.0113$, $\mathfrak{m}_{12} = 0.0014$ and $\mathfrak{m}_{22} = 0.0135$. In this case, $\mathfrak{R}_{\star}^{\Sigma} = 0.0032 > 0$.

*Scenario 1: Disappearance of bacteria*

Again, if we select the parameters values from Table 3 (Scenario 1), then the result is

$$\begin{aligned}\mathfrak{R}_{\star}^{\Sigma} &= \mathfrak{b}\int_{\mathbb{R}_+} \mathcal{G}(y,0)\pi^{\mathbf{U}}(\mathrm{d}y) - \mathcal{Q}_1 - 0.5\mathfrak{m}_{20}^2 \\ &= \lim_{T\to\infty} T^{-1}\int_0^T \frac{\mathfrak{b}\mathbf{U}(\tau)}{1+\mathfrak{K}_{\mathbf{N}}\mathbf{U}(\tau)}\mathrm{d}\tau - \mathcal{Q}_1 - 0.5\mathfrak{m}_{20}^2 = -0.0511 < 0.\end{aligned}$$

Theoretically, we have the disappearance of the bacteria **M** according to Theorem 2.1. It remains to verify it numerically. From Fig. 6, the bacteria will clear up in about five days with long-term persistence of **N**.

*Scenario 2: Continuation of bacteria*

Now, if we select the parameters values from Table 3 (Scenario 2), then we get

$$\begin{aligned}\mathfrak{R}_{\star}^{\Sigma} &= \mathfrak{b}\int_{\mathbb{R}_+} \mathcal{G}(y,0)\pi^{\mathbf{U}}(\mathrm{d}y) - \mathcal{Q}_1 - 0.5\mathfrak{m}_{20}^2 \\ &= \lim_{T\to\infty} T^{-1}\int_0^T \frac{\mathfrak{b}\mathbf{U}(\tau)}{1+\mathfrak{K}_{\mathbf{N}}\mathbf{U}(\tau)}\mathrm{d}\tau - \mathcal{Q}_1 - 0.5\mathfrak{m}_{20}^2 = 0.0032 > 0.\end{aligned}$$

From Theorem 2.1, we establish that there is a single stable distribution for (3.3) which is depicted in Fig. 7. In this figure, we remark also the persistence of all classes.

**Remark 3.2.** From Figs. 2, 4 and 6, we emphasize that heavy fluctuations have a passive influence on the time extinction of the disease.

## Conclusion

This research proposed a new approach to deal with an industrial wastewater model with strong fluctuations. Explicitly, we have proposed and treated a new form of the chemostat system which integrates two improvements: general response function and polynomial white noises. This fusion offers a global view of the interaction between the different elements of the chemostat process in a highly disturbed environment. The outcomes of this part can be summarized as follows:

- We have given the global threshold of our model based on some dynamical properties of an auxiliary Markov process **U** perturbed by polynomial perturbations.
- In Theorem 2.1, we have studied the extinction case and the weak convergence of the distribution of **N** to that of **U**.
- In Theorem 2.2, we have proved the stationarity and ergodicity of our system. It should be mentioned that the analysis of these two properties is very significant for perturbed systems. Especially, in the case of chemostat models, the ergodicity offers a general idea of the bacteria permanence.

Numerically, we have chosen the first three values of $H$, that are, linear, quadratic and cubic cases. Our main objective was to verify the sharpness of the proposed threshold. For this cause, we have selected appropriate parameter values that give an amount of $\mathfrak{R}_{\star}^{\Sigma}$ close to zero in both sides. From numerical outcomes, we have emphasized that $\mathfrak{R}_{\star}^{\Sigma}$ is the real sill of the model (1.3) in the three studied cases. What caught our attention is that when we increase the order of the disturbance, the bacteria extinction time decreases. That is, strong fluctuations have a passive influence on the duration of the chemostat process.

In general, we point out that this study generalizes many previous works to the case of general perturbation. Furthermore, it offers new insights into understanding wastewater mechanisms with complex real-world assumptions. In other words, the approach proposed in this article leaves many research avenues to be explored in future works.

## CRediT authorship contribution statement

**Yassine Sabbar:** Conceptualization, Software, Writing manuscript. **Anwar Zeb:** Writing – reviewing final manuscript. **Driss Kiouach:** Methodology. **Nadia Gul:** Review, Data collection, Graphs sketching. **Thanin Sitthiwirattham:** Funding, Visualization. **Dumitru Baleanu:**

Supervision, Investigation. **Jiraporn Pongsopa:** Funding, Review final manuscript, Validation.

## Declaration of competing interest

The authors declare that they have no known competing financial interests or personal relationships that could have appeared to influence the work reported in this paper.

## Data availability

No data was used for the research described in the article.

## Acknowledgment

This project is funded by National Research Council of Thailand (NRCT) and Suan Dusit University, Thailand: N42A650384.

## References

[1] Smith H, Waltman P. The theory of the chemostat: Dynamics of microbial competition. Cambridge University Press; 1995.
[2] Nazaroff W, Alvarez-Cohen L. Environmental engineering science. John Wiley and Sons; 2001.
[3] Novick A, Szilard L. Experiments with the chemostat on spontaneous mutations of bacteria. Proc Natl Acad Sci 1950;36(12):708–19.
[4] Novick A, Szilard L. Description of the chemostat. Science 1950;112:715–6.
[5] Pavlou S, Kevrekidis I. Microbial predation in a periodically operated chemostat: A global study of the interaction between natural and externally imposed frequencies. Math Biosci 1992;108(1):1–55.
[6] Fergola P, Tenneriello C, Ma Z, Wen X. Effects of toxicants on chemostat models. Cybern Syst 1994;94:887–94.
[7] Nelson M, Sidhu H. Reducing the emission of pollutants in food processing wastewaters. Chem Eng Process: Process Intensif 2007;46(5):429–36.
[8] Beran B, Kargi F. A dynamic mathematical model for wastewater stabilization ponds. Ecol Model 2005;181(1):39–57.
[9] Shakeri H, Motiee H, McBean E. Forecasting impacts of climate change on changes of municipal wastewater production in wastewater reuse projects. J Cleaner Prod 2021;329:129790.
[10] Lv J, Fu M, Gan J, Cao Y, Xiao F. Study on the treatment of tempering lubricant wastewater in steel industry by anaerobic aerobic process. J Cleaner Prod 2022;2022:131754.
[11] Lahlou FZ, Mackey HR, Al-Ansari T. Role of wastewater in achieving carbon and water neutral agricultural production. J Cleaner Prod 2022;2022:130706.
[12] Nazaroff W, Alvarez-Cohen L. Environmental engineering science. John Wiley and Sons; 2001.
[13] Liu X, Wang D, Li A. Biodiesel production of Rhodosporidium toruloides using different carbon sources of sugar-containing wastewater: Experimental analysis and model verification. J Cleaner Prod 2021;323:129112.
[14] Marichamy MK, Kumaraguru A, Jonna N. Particle size distribution modeling and kinetic study for coagulation treatment of tannery industry wastewater at response surface optimized condition. J Cleaner Prod 2021;297:126657.
[15] Kumar P, Erturk VS. Environmental persistence influences infection dynamics for a butterfly pathogen via new generalised Caputo type fractional derivative. Chaos Solitons Fractals 2021;144:110672.
[16] Nabi KN, Kumar P, Erturk VS. Projections and fractional dynamics of COVID-19 with optimal control strategies. Chaos Solitons Fractals 2021;145:110689.
[17] Abboubakar H, Kumar P, Erturk VS, Kumar A. A mathematical study of a tuberculosis model with fractional derivatives. Int J Model Simul Sci Comput 2021;12(04):2150037.
[18] Nguyen DH, Nguyen NN, Yin G. General nonlinear stochastic systems motivated by chemostat models: Complete characterization of long time behavior, optimal controls, and applications to wastewater treatment. Stochastic Process Appl 2020;130:4608–42.
[19] Butler G, Wolkowicz G. A mathematical model of the chemostat with a general class of functions describing nutrient uptake. SIAM J Appl Math 1985;45(1):138–51.
[20] Dong Q, Ma W, Sun M. The asymptotic behavior of a chemostat model with Crowley-Martin type functional response and time delays. J Math Chem 2013;51(5):1231–48.
[21] Li H, Wu J, Li Y, Liu C. Positive solutions to the unstirred chemostat model with Crowley-Martin functional response. J Math Chem 2018;23(8):2951.
[22] Li B. Global asymptotic behavior of the chemostat: General response functions and different removal rates. SIAM J Appl Math 1998;59(2):411–22.
[23] Tang B, Wolkowicz G. Mathematical models of microbial growth and competition in the chemostat regulated by cell-bound extracellular enzymes. J Math Biol 1992;31(1):1–23.
[24] Goel NS, Dyn NR. Stochastic models in biology. Elsevier; 2016.
[25] Kiouach D, Sabbar Y, El-idrissi SEA. New results on the asymptotic behavior of an SIS epidemiological model with quarantine strategy, stochastic transmission, and Levy disturbance. Math Methods Appl Sci 2021;44(17):13468–92.
[26] Kiouach D, Sabbar Y. Developing new techniques for obtaining the threshold of a stochastic SIR epidemic model with 3-dimensional Levy process. J Appl Nonlinear Dyn 2022;11(2):401–14.
[27] Kiouach D, Sabbar Y. The long-time behaviour of a stochastic SIR epidemic model with distributed delay and multidimensional levy jumps. Int J Biomath 2021;2021:2250004.
[28] Kiouach D, Sabbar Y. Dynamic characterization of a stochastic SIR infectious disease model with dual perturbation. Int J Biomath 2021;14(4):2150016.
[29] Kiouach D, Sabbar Y. Ergodic stationary distribution of a stochastic Hepatitis B epidemic model with interval-valued parameters and compensated Poisson process. Comput Math Methods Med 2020;2020:9676501.
[30] Winkelmann S, Schutte C. Stochastic dynamics in computational biology. Springer; 2020.
[31] Kiouach D, Sabbar Y. Stability and threshold of a stochastic SIRS epidemic model with vertical transmission and transfer from infectious to susceptible individuals. Discrete Dyn Nat Soc 2018;2018:1–13.
[32] Sabbar Y, Kiouach D, Rajasekar S, El-idrissi SA. The influence of quadratic levy noise on the dynamic of an SIC contagious illness model: New framework, critical comparison and an application to COVID-19 (SARS-CoV-2) case. Chaos Solitons Fractals 2022;159(2022):112110.
[33] Wilkinso D. Stochastic modelling for systems biology. Chapman and Hall-CRC; 2006.
[34] Kiouach D, Sabbar Y. Threshold analysis of the stochastic Hepatitis B epidemic model with successful vaccination and levy jumps. In: 4th world conference on complex systems, vol. 2019. IEEE; 2019, p. 1–6.
[35] Sabbar Y, Kiouach D, Rajasekar SP. Acute threshold dynamics of an epidemic system with quarantine strategy driven by correlated white noises and Lévy jumps associated with infinite measure. Int J Dynam Control 2022;2022:1–14.
[36] Sabbar Y, Din A, Kiouach D. Predicting potential scenarios for wastewater treatment under unstable physical and chemical laboratory conditions: A mathematical study. Results Phys 2022;39:105717.
[37] Matis JH, Zheng Q, Kiffe TR. Describing the spread of biological populations using stochastic compartmental models with births. Math Biosci 1995;126(2):215–47.
[38] Faddy M. Nonlinear stochastic compartmental models. Math Med Biol: J IMA 1985;2(4):287–97.
[39] Kiouach D, Sabbar Y. The threshold of a stochastic SIQR epidemic model with levy jumps. In: Trends in biomathematics: Mathematical modeling for health, harvesting, and population dynamics, vol. 2019. 2019, p. 87–105.
[40] Ditlevsen S, Samson A. Introduction to stochastic models in biology. In: Stochastic biomathematical models, vol. 2013. 2013, p. 3–35.
[41] Ji C, Jiang D, Shi N. The behavior of an SIR epidemic model with stochastic perturbation. Stoch Anal Appl 2012;30(5):755–73.
[42] Zhang XB, Huo HF, Xiang H, Shi Q, Li D. The threshold of a stochastic SIQS epidemic model. Physica A 2017;482:362–74.
[43] Zhao Y, Jiang D. The threshold of a stochastic SIS epidemic model with vaccination. Appl Math Comput 2014;243:718–27.
[44] Liu XQ, Zhong SM, Tian BD, Zheng FX. Asymptotic properties of a stochastic predator-prey model with Crowley-Martin functional response. J Appl Math Comput 2013;43(1):479–90.
[45] Liu Q, Jiang D, Hayat T, Alsaedi A. Dynamics of a stochastic predator–prey model with stage structure for predator and Holling type II functional response. J Nonlinear Sci 2018;28(3):1151–87.
[46] Liu Q, Jiang D. Influence of the fear factor on the dynamics of a stochastic predator-prey model. Appl Math Lett 2021;112:106756.
[47] Liu Q, Jiang D, Shi N, Hayat T, Alsaedi A. Stationarity and periodicity of positive solutions to stochastic SEIR epidemic models with distributed delay. Discrete Contin Dyn Syst Ser B 2017;22(6):2479.
[48] Kar T, Nandi S, Jana S, Mandal M. Stability and bifurcation analysis of an epidemic model with the effect of media. Chaos Solitons Fractals 2019;120:188–99.
[49] Liu Q, Jiang D. Stationary distribution and extinction of a stochastic SIR modelwith nonlinear perturbation. Appl Math Lett 2017;73:8–15.
[50] Lu C, Sun G, Zhang Y. Stationary distribution and extinction of a multi stage HIV model with nonlinear stochastic perturbation. J Appl Math Comput 2021;2021.
[51] Liu Q. Dynamics of a stochastic SICA epidemic model for HIVtransmission with higher order perturbation. Stoch Anal Appl 2021;2021.
[52] Rajasekar SP, Pitchaimani M, Zhu Q. Higher order stochastically perturbed SIRS epidemic model with relapse and media impact. Math Methods Appl Sci 2021;2021:1–21.
[53] Weiwei Z, Xinzhu M, Yulin D. Periodic solution and ergodic stationary distribution of stochastic SIRI epidemic systems with nonlinear perturbations. J Syst Sci Complex 2019;32:1104–24.
[54] Liu Q, Jiang D. Dynamical behavior of a higher order stochastically perturbed HIV-AIDS model with differential infectivity and amelioration. Chaos Solitons Fractals 2020;141:110333.

[55] Han B, Jiang D, Hayat T, Alsaedi A, Ahmed B. Stationary distribution and extinction of a stochastic staged progression AIDS model with staged treatment and second-order perturbation. Chaos Solitons Fractals 2020;140:110238.
[56] Liu Q, Jiang D, Hayat T, Alsaedi A, Ahmed B. Dynamical behavior of a higher order stochastically perturbed SIRI epidemic model with relapse and media coverage. Chaos Solitons Fractals 2020;139:110013.
[57] Lv X, Meng X, Wang X. Extinction and stationary distribution of an impulsive stochastic chemostat model with nonlinear perturbation. Chaos Solitons Fractals 2018;110:273–9.
[58] Liu Q, Jiang D, Hayat T, Alsaedi A. Stationary distribution of a regime switching predator prey model with anti predator behaviour and higher order perturbations. Physica A 2019;515:199–210.
[59] Liu Q, Jiang D, Hayat T, Alsaedi A. Long-time behavior of a stochastic logistic equation with distributed delay and nonlinear perturbation. Physica A 2018;508:289–304.
[60] Liu Q, Jiang D, Hayat T, Ahmed B. Periodic solution and stationary distribution of stochastic SIR epidemic models with higher order perturbation. Physica A 2017;482:209–17.
[61] Zu L, Jiang D, ORegan D, Hayat T, Ahmed B. Ergodic property of a Lotka Volterra predator prey model with white noise higher order perturbation under regime switching. Appl Math Comput 2018;330:93–102.
[62] Liu Q, Jiang D, Hayat T, Ahmed B. Stationary distribution and extinction of a stochastic predator prey model with additional food and nonlinear perturbation. Appl Math Comput 2018;320:226–39.
[63] Liu Q, Jiang D. Dynamical behavior of a stochastic multigroup staged-progression HIV model with saturated incidence rate and higher-order perturbations. Int J Biomath 2021;17(7):2150051.
[64] Zhou B, Han B, Jiang D, Hayat T. Ergodic stationary distribution and extinction of a hybrid stochastic SEQIHR epidemic model with media coverage, quarantine strategies and pre existing immunity under discrete Markov switching. Appl Math Comput 2021;410:126388.
[65] Zhou B, Han B, Jiang D. Ergodic property, extinction and density function of a stochastic SIR epidemic model with nonlinear incidence and general stochastic perturbations. Chaos Solitons Fractals 2021;152:111338.
[66] Ikeda N, Watanabe S. A comparison theorem for solutions of stochastic differential equations and its applications. Osaka J Math 1977;14(3):619–33.
[67] Mao X. Stochastic differential equations and applications. Elsevier; 2007.
[68] Tong J, Zhang Z, Bao J. The stationary distribution of the facultative population model with a degenerate noise. Statist Probab Lett 2013;83(2):655–64.
[69] Zhao D, Yuan S. Sharp conditions for the existence of a stationary distribution in one classical stochastic chemostat. Appl Math Comput 2018;339:199–205.